Technical, economic and environmental analysis of solar thermochemical production of drop-in fuels

Journal Article

Author(s):
Moretti, Christian [ID]; Patil, Vikas; Falter, Christoph; Geissbühler, Lukas; Patt, Anthony; Steinfeld, Aldo [ID]

Technical, economic and environmental analysis of solar thermochemical production of drop-in fuels

Christian Moretti [a,*], Vikas Patil [b,1], Christoph Falter [c], Lukas Geissbühler [c], Anthony Patt [a], Aldo Steinfeld [b]

[a] ETH Zurich, Department of Environmental Systems Science, 8092 Zürich, Switzerland
[b] ETH Zurich, Department of Mechanical and Process Engineering, 8092 Zurich, Switzerland
[c] Synhelion SA, Lugano, Switzerland

HIGHLIGHTS

- Techno-economic assessment of industrial-scale production of solar thermochemical fuels.
- Round-the-clock continuous cycle operation driven by concentrated solar heat supplemented by thermal energy storage.
- Jet fuels can be produced from sunlight and air for 2.5 €/L in the future and can reach 0.6–1.3 €/L in the long term.
- Greenhouse gas savings exceed 70 % for fuels and locations considered.

GRAPHICAL ABSTRACT
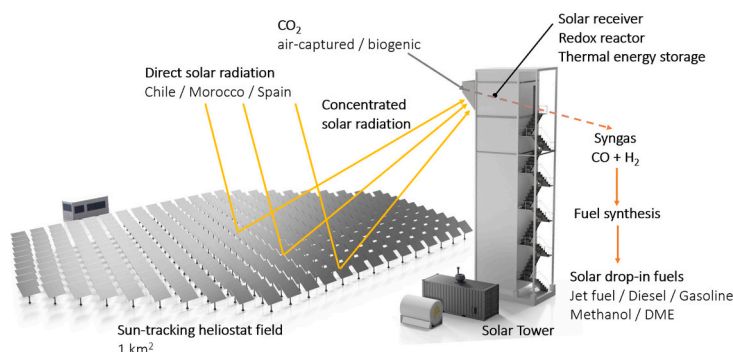
ABSTRACT

This study analyzes the technical performance, costs and life-cycle greenhouse gas (GHG) emissions of the production of various fuels using air-captured water and CO_2, and concentrated solar energy as the source of high-temperature process heat. The solar thermochemical fuel production pathway utilizes a ceria-based redox cycle for splitting water and CO_2 to syngas – a tailored mixture of H_2 and CO – which in turn is further converted to liquid hydrocarbon fuels. The cycle is driven by concentrated solar heat and supplemented by a high-temperature thermal energy storage for round-the-clock continuous operation. The study examines three locations with high direct normal irradiation using a baseline heliostat field reflective area of 1 km^2 for the production of six fuels, i.e. jet fuel and diesel via Fischer-Tropsch, methanol, gasoline via methanol, dimethyl ether, and hydrogen. Two scenarios are considered: near-term future by the year 2030 and long-term future beyond 2030.

In the near-term future in Sierra Gorda (Chile), the minimum fuel selling price is estimated at around 76 €/GJ (2.5 €/L) for jet fuel and diesel, 65 €/GJ for methanol, gasoline (via methanol) and dimethyl ether (DME), and 42 €/GJ for hydrogen (excluding liquefaction). In the long-term future, with advancements in solar receiver, redox reactor, high-temperature heat recovery and direct air capture technologies, the industrial-scale plant could

* Corresponding author.
  E-mail address: christian.moretti@usys.ethz.ch (C. Moretti).
[1] Current affiliation.

achieve a solar-to-fuel efficiency up to 13–19 %, depending on the target fuel, resulting in a minimum fuel selling price of 16–38 €/GJ (0.6–1.3 €/L) for jet fuel and diesel, and 14–32 €/GJ for methanol, gasoline, and DME, making these fuels synthesized from sunlight and air cost-competitive vis-à-vis e-fuels. To produce the same fuels in Tabernas (Spain) and Ouarzazate (Morocco) as in Sierra Gorda, the production cost would increase by 22–33 %. Greenhouse gas savings can be over 80 % already in the near-term future.

1. Introduction

The transition towards climate-neutral transportation requires the world to seek innovative solutions to mitigate climate change impacts and reduce dependence on fossil fuels. Renewable fuels, currently mostly biofuels (Callegari et al., 2020; O'Connell et al., 2019), have emerged as a promising solution for decarbonizing the transportation sector. Biofuels reached a record production volume of 163 billion L in 2019, with a 70 % share made of ethanol, whose production is dominated by US corn-derived ethanol and Brazilian sugar cane-derived ethanol (IEA, 2020; Renewable fuels association, 2022). However, constraints in feedstock availability, limited greenhouse gas (GHG) emissions savings and other environmental concerns, e.g. land use changes, limit further upscaling of biofuels (de Jong et al., 2015; Escobar and Laibach, 2021). Thus, a complementary solution to biofuels with greater scalability and climate change mitigation potential is urgently required to reduce fossil fuel demand globally and, simultaneously, global climate change mitigation targets. Solar energy and air are attractive and practically unlimited resources. Solar energy technologies such as photovoltaics and concentrating solar thermal convert solar irradiation into electricity and process heat, and have experienced a continued cost decrease in the last two decades (He et al., 2020; Lilliestam et al., 2017). At the same time, the first commercial direct air capture (DAC) plants removing carbon dioxide directly from the air started operations (Climeworks, 2022). The combination of cheaper renewables and the expected fast cost decrease of DAC has given synthetic hydrocarbon fuels increased attention with minimum yearly targeted production volumes introduced in the European Union (EU) legislation (EU, 2023).

Fischer-Tropsch (FT) and methanol syntheses are established gas-to-liquid (GTL) processes for the synthesis of renewable transportation fuels (Poluzzi et al., 2022). Both use syngas – a specific mixture of hydrogen (H_2) and carbon monoxide (CO) – as the precursor. There are several ways to produce the syngas needed for the FT/methanol synthesis, e.g. via biomass gasification, water electrolysis and reverse water-gas shift reaction (RWGS), or via solar thermochemical splitting of CO_2 and water. The latter has the potential to reach high solar-to-syngas energy conversion efficiencies due to its use of the full solar spectrum (Falter et al., 2020; Schäppi et al., 2022; Zoller et al., 2022) and offers more thermal energy integration synergies with the adsorption-desorption DAC (Prats-Salvado et al., 2021). In contrast, e-fuels produced via power-to-liquid pathways require renewable electricity to produce excess hydrogen via water electrolysis (Marchese et al., 2022), of which a significant portion is consumed by the highly endothermic RWGS reaction for producing the CO component of syngas.

A few preliminary studies have already shown promising production costs and climate change advantages of jet fuels via the solar thermochemical pathway utilizing CO_2 from DAC (Falter et al., 2020; Falter and Sizmann, 2022; Prats-Salvado et al., 2022). This study presents a techno-economic analysis of various fuels from air and sunlight produced via an industrial-scale thermochemical redox cycle relying on ceria to split H_2O and CO_2. The fuel plant is designed to operate continuously, round-the-clock, by relying on thermal energy storage as well as on thermal management to operate in an energetically self-sufficient way. Such a design is novel and, as shown in our analysis, has significant advantages when integrating the GTL.

We assess the production of jet fuel, diesel, methanol, gasoline (via methanol), dimethyl ether (DME) and hydrogen in terms of techno-economic viability and environmental sustainability. Economic viability is assessed in terms of the so-called minimum fuel selling price (MFSP). The MFSP indicates the minimum price to sell the renewable fuel to recover fuel production costs. Sustainability is evaluated in terms of life cycle GHG mitigation potential when replacing traditional fossil fuels. In the EU, to be considered sustainable, fuels from CO_2 must comply with the EU Renewable Energy Directive (RED II) 70 % GHG reduction criterion (EC, 2018). Our analysis looks at two time horizons, i.e. near-term future (fuel plant built by 2030) and long-term future (fuel plant built in the 2030s decade).

The end use of the fuel is assumed to take place in Europe. Our analysis investigates three production sites with high direct normal solar irradiation (DNI), i.e. Tabernas (Spain), Sierra Gorda (Chile) and Ouarzazate (Morocco). Owing to their high DNI, these three locations already have operational concentrating solar power (CSP) plants.[2] Hour-wise DNI is used to calculate the energy and mass balance of the fuel production plant for each location for every hour of a typical year. The hour-wise technical modelling approach enables the sizing of key components for adequately determining their costs and material requirements, e.g. the solar receiver, redox reactor and thermal energy storage units.

2. Model description

A system-level model was developed for the fuel plant's technical, economic and environmental sustainability assessment. The analysis looks at near-term future and the long-term future, and three different production sites, i.e. Sierra Gorda, Tabernas and Ouarzazate. Mass and energy balances were calculated for each location with hour-wise modelling. This section is organized as follows. Section 2.1 presents the plant schematic and describes the solar thermochemical fuel pathway. Subsequent sections describe the method, assumptions and data used for the technical model (Section 2.2), the economic model (Section 2.3), and the environmental sustainability model (Section 2.4).

2.1. Plant schematic

Fig. 1 shows a simplified schematic of the industrial-scale fuel production plant using the solar thermochemical pathway.

The two main ingredients of this pathway, i.e. H_2O and CO_2, are captured by the DAC process. In our study, we assume a low-temperature adsorption process. This DAC process, based on an adsorption-desorption cyclic process (Wurzbacher et al., 2012), integrates well with a solar thermochemical redox cycle (1000–1900 K) driven by concentrated solar heat, which can supply waste heat at 90–100 °C (Prats-Salvado et al., 2021). Furthermore, the choice of low-temperature DAC also reflects the first type of DAC process that has reached large-scale commercial applications (Climeworks, 2022). The solar concentrating system consists of a field of sun-tracking heliostats that reflect and concentrate DNI onto an array of solar receivers on the top of a tower. The solar receivers convert concentrated solar radiation

---

[2] Sierra Gorda is near the site of the Cerro Dominador solar tower CSP plant. Tabernas is the site of two solar tower facilities of the Centro de Investigaciones Energéticas, Medioambientales y Tecnológicas (CIEMAT) Plataforma Solar de Almería research institute. Ouarzazate is the site of the Noor solar tower CSP plant.
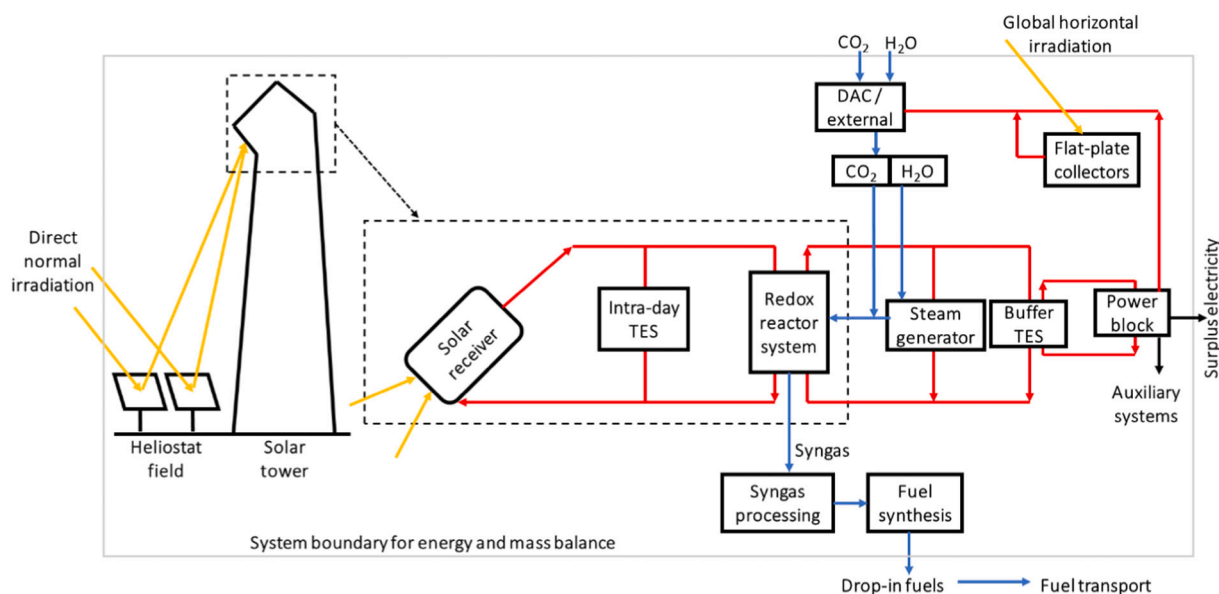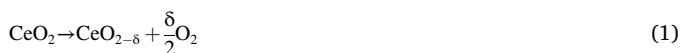
Fig. 1. Simplified schematic of the industrial-scale fuel production plant using the solar thermochemical pathway. Solar irradiation indicated in yellow, heat flows in red, mass flows in blue, and electrical power in black.

into high-temperature (>1500 °C) process heat that is delivered to a redox reactor, wherein H_2O and CO_2 are split to H_2 and CO. The redox cycle comprises two steps.

$$CeO_2 \rightarrow CeO_{2-\delta} + \frac{\delta}{2}O_2 \quad (1)$$

$$CeO_{2-\delta} + \delta CO_2 \rightarrow CeO_2 + \delta CO \quad (2)$$

$$CeO_{2-\delta} + \delta H_2O \rightarrow CeO_2 + \delta H_2 \quad (3)$$

Firstly, in the endothermic stage (Eq. (1)), ceria is thermally reduced and releases oxygen O_2. Secondly, in the exothermic stage, the reduced ceria is re-oxidized by CO_2 (Eq. (2)) and/or H_2O (Eq. (3)) to yield CO and/or H_2, respectively.

Depending on the targeted fuel, the syngas needs to be processed differently before GTL processing. In the Fischer-Tropsch (FT) synthesis, various fuels are produced at the same time. The production of diesel or jet fuel is commonly maximized (Kreutz et al., 2020). The production of the targeted FT fuel also results in the co-production of gasoline/naphtha. Methanol is produced by converting syngas via methanol synthesis (Poluzzi et al., 2022). Methanol can be blended with gasoline, used as a feedstock for further gasoline production, or used directly in specially tuned engines. Methanol-to-gasoline (MTG) is produced by first converting syngas to methanol, followed by its dehydration to dimethyl ether (DME) and eventual reduction to gasoline (Trinca et al., 2023). DME can be blended with diesel or used directly in specially tuned engines. An important feature of the thermochemical redox cycle is that the syngas composition, especially the molar ratios H_2:CO and CO:CO_2, can be controlled by adjusting the H_2O:CO_2 feed ratio and/or by performing the splitting of CO_2 and H_2O separately. In either case, the syngas purity and quality are suitable for GTL processing and can be tailored for methanol or FT synthesis without additional steps for correcting composition and/or separating undesired by-products (Schäppi et al., 2022). When the targeted fuel is hydrogen, the process does not require CO_2 and, therefore, does not rely on DAC but only on water supply. Water is then split in the redox reactor to form hydrogen directly.

2.2. Technical model

The technical model calculates the energy and mass flows of the fuel

Table 1
Major inputs to the technical model. Same values are used for near-term future and long-term future scenarios unless specified otherwise. Sources and justification of values are discussed in the main text.

Technical model input	Unit	Value
Heliostat field reflective area	km^2	1
Heliostat field optical efficiency (annual average)	–	0.65
Receiver thermal efficiency	–	0.65 (near-term future), 0.75 (long-term future)
Intra-day TES round-trip efficiency	–	0.81
Redox reactor reduction temperature	°C	1500
Redox reactor reduction pressure	bar (abs)	0.01
Redox reactor oxidation temperature	°C	727 (1000 K)
Redox reactor oxidation pressure	bar (abs)	10
Redox reactor heat losses	%	10
Redox reactor heat-to-syngas efficiency	–	0.30 (near-term future), 0.55 (long-term future)
CO_2-to-CO conversion	–	0.50 (FT synthesis), 0.60 (methanol synthesis)
H_2O-to-H_2 conversion	–	0.50
H_2:CO_x molar ratio in produced syngas	–	2.1 (FT synthesis), 2.4 (methanol synthesis)
DAC heat demand	kJ_{th}/mol_{CO_2}	524.1 (near-term future), 237.6 (long-term future)
DAC electricity demand	kJ_e/mol_{CO_2}	110.9 (near-term future), 79.2 (future)
Power block heat-to-electricity efficiency	–	0.40

plant to serve as the basis for the economic and life-cycle GHG assessments. The model consists of inter-connected systems, whose performance is estimated using data and correlations from the literature, as described further, summarized in Table 1, and also illustrated further in Fig. A.1.

Heliostat field – A baseline heliostat field reflective area of 1 km^2 is assumed as an industrial-scale plant. Hour-wise DNI for the three chosen locations was obtained from a solar radiation model based on satellite imaging, validated with ground measurements at various locations worldwide (EC JRC, 2023). The energy and mass flows of

the plant are thus calculated for every hour of the year. A heliostat field optical efficiency determines the portion of the DNI, which is incident and reflected by the heliostat field, that reaches the apertures of the solar receivers on top of the solar tower, accounting for optical losses along the path, such as mirror's reflectivity, tracking accuracy, atmospheric attenuation, blocking/shadowing, and cosine losses. Depending on the location, field layout, tower height and utilization of radiation spillage around the receiver aperture, the theoretically maximum heliostat field optical efficiency can be up to 0.70 (Corsi et al., 2022). The value of 0.65 is chosen for the near-term as well as long-term scenarios.

Solar receiver – There are currently no industrial-scale installations and only a handful of lab-scale prototypes for solar receivers supplying process heat up to and beyond 1500 °C to drive the ceria-based redox cycle. A novel approach to high-temperature solar receivers is considered in this study, proposed by Ambrosetti and Good (2019), experimentally demonstrated (Good et al., 2020), and under further development and scale-up at Synhelion SA. The receiver consists of a cavity, carrying steam at near-ambient pressure, bounded by black walls and a windowless aperture with a gas curtain to contain the steam. Concentrated solar radiation entering through the aperture gets absorbed by the cavity walls, steam being largely transparent in the visible wavelength range. The cavity walls heat up and emit thermal radiation, which the steam absorbs, thus producing high-temperature process heat. Such a configuration exploits the ability of steam, among other molecular gases, to absorb a major fraction of infrared radiation while being mostly transparent to the visible range of solar radiation. A receiver's thermal efficiency of 0.65 is assumed in this analysis, defined as the ratio of the enthalpy gain of steam across the receiver from 1400 °C to 1500 °C, over the solar energy input through the aperture (Ambrosetti and Good, 2019). This definition takes into account all radiative, conductive and convective heat losses in the solar receiver and can be directly multiplied by the heliostat's optical efficiency to obtain the solar-to-heat energy efficiency of the solar concentrating system delivering steam at 1500 °C. It is assumed that with variable DNI over the course of a day, the heliostat field focuses on a variable number of receivers, maintaining a mean solar flux density of 1200 kW/m^2 over each receiver aperture to deliver steam at a constant temperature.

Intra-day thermal energy storage (TES) – The technology for TES is based on a thermocline-packed bed of ceramics (Geissbühler, 2017; Lidor et al., 2023; Zanganeh et al., 2012). Process heat delivered by the receiver is distributed between driving the redox reactor system directly and charging the intra-day TES, which operates between 1400 °C and 1500 °C, similar to the receiver. The intra-day TES stores surplus solar heat during periods of high DNI and drives the redox reactor system, partially or fully, during periods of low or no DNI. A round-trip (charging-discharging) efficiency of 0.81 is assumed to account for the heat losses to the surroundings (Geissbühler, 2017; Lidor et al., 2023; Zanganeh et al., 2012). The thermal storage medium is assumed to be alumina- or mullite-based. As a trade-off between cost and extending operating hours, the maximum capacity of the intra-day TES is set to the thermal energy required to drive the whole fuel plant for 24 h, including auxiliary systems. Depending on the location, heliostat field size and auxiliary energy demand, the energy stored in the TES will not always reach this maximum capacity during the year. If it does, the surplus energy is assumed to be dumped.

Redox reactor system – A ceria-based, dual-storage reactor system enables the recovery of the sensible heat rejected during the temperature swing between the reduction step (1500 °C) and oxidation step (727 °C) of ceria and of the heat released during the exothermic oxidation of ceria (Falter et al., 2020; Geissbühler, 2017; Lidor et al., 2023). 10 % of the thermal energy supplied to the redox reactor system is assumed lost to the surroundings. The extent of ceria non-stoichiometry (δ in Eq. (1)) is calculated for the reduction and

oxidation temperatures and pressures assuming thermodynamic equilibrium (Panlener et al., 1975), which in turn yields the maximum possible syngas output (CO and H_2 in Eqs. (2) and (3)) per mol of ceria. The heat-to-syngas efficiency of the reactor is defined as the ratio of the higher heating value (HHV) of the produced syngas (CO + H_2) to the net heat input to the reactor (after applying the heat losses). For the reaction conditions given in Table 1, the theoretically maximum possible heat-to-syngas efficiency is 0.61, when heat recovery between the reduction and oxidation steps is perfect and the only heat input required to drive the redox cycle is the enthalpy change of reduction (Eq. (1)), $\Delta H° \approx 475$ kJ per ½ mol O_2. The balance of energy in this ideal system is the heat released by the exothermic oxidation step at 727 °C (Falter et al., 2020), which cannot be utilized for sensible heating of ceria or for the endothermic reduction step occurring at higher temperatures. In a real system, besides heat losses to the environment, heat recovery will be imperfect. A conservative value of 0.30 for the heat-to-syngas efficiency is thus assumed for the Near-term future case, while an optimistic value of 0.55 is used for the Long-term future case, assuming advances in high-temperature heat recovery methods (Geissbühler, 2017; Lidor et al., 2023). Thermal energy at below 727 °C is recovered and utilized for pre-heating CO_2 and H_2O and fulfilling auxiliary systems' heat and electrical energy demands.

Syngas processing – The quantity of CO_2 and H_2O required is back-calculated by assuming a set H_2:CO_x molar ratio in the produced syngas, CO_2-to-CO conversion, and H_2O-to-H_2 conversion, together with the heat-to-syngas efficiency and calorific values of H_2 and CO (Table 1). Unreacted H_2O at the reactor exit is condensed out and recycled back to the H_2O input into the reactor. Unreacted CO_2 is separated for FT synthesis (not separated for methanol synthesis, thus also for MTG gasoline and DME) using an absorption process relying on monoethanolamine (MEA) and is recycled back to the CO_2 input into the reactor. Based on the target fuel, produced syngas, with or without CO_2, is compressed to 25 bar (abs.) for methanol or FT synthesis.

CO_2 and H_2O source – As unreacted CO_2 and H_2O are separated and recycled back to the reactor inputs, the CO_2 and H_2O sources only supply the net requirement. When DAC is taken as the CO_2 source, it is assumed that H_2O is co-captured at an H_2O:CO_2 molar ratio of 2.41, sufficient to produce the required H_2:CO_x ratio of 2.1 for FT synthesis (2.4 for methanol synthesis). The DAC system is represented by the electrical and thermal energy demand per mole of CO_2 captured, which includes the energy spent in co-capturing and separating H_2O (Deutz and Bardow, 2021). If CO_2 is sourced externally, no energy requirement for its capture is assumed. H_2O is assumed to be sourced externally as well.

Fuel synthesis – The fuel synthesis system is represented by a mass or molar balance, depending on the target fuel. A mass balance is applied for FT synthesis due to the wide spectrum of hydrocarbons formed. The product mass distribution to produce on-specification fuels, i.e. fulfilling fuel standards to enable their drop-in use in jet and motor engines, is based on de Klerk (2011). Tuning the FT synthesis to maximize jet fuel production results in the co-production of a smaller quantity of gasoline. Similarly, tuning the FT synthesis to maximize diesel production co-produces gasoline and jet fuel. A molar balance is applied for methanol synthesis due to the typically high selectivity of the catalyst towards methanol formation (>99 %). A further molar balance is applied to produce DME from methanol, while a mass balance is applied to produce gasoline from methanol (MTG). A significant quantity of H_2O is formed in the fuel synthesis processes and is recycled back into the H_2O input into the reactor. The heat released during the exothermic FT and methanol syntheses is assumed to be utilized for endothermic, post-treatment of the products to obtain on-specification fuels.

Auxiliary systems – The electrical energy demand of the auxiliary systems (mainly reactor vacuum pump, DAC system, various

compressors and pumps) is fulfilled by a power block, driven by the high-temperature heat recovered from the redox reactor system and stored in a medium-temperature (<700 °C) buffer TES unit. The power block is based on the conventional steam Rankine cycle with an assumed heat-to-electricity efficiency of 0.40. The thermal energy demand of the auxiliary system consists of a high-temperature portion (for heating up CO_2 and H_2O to reduction temperature), also fulfilled by the high-temperature heat recovered from the redox reactor system, and if necessary, supplemented by the high-temperature solar heat supplied directly by the receiver or intra-day TES. Waste heat from the power block, i.e. from its condenser, is utilized to fulfil the heat demand of the DAC system, which requires a low-temperature heat source at about 100 °C (Deutz and Bardow, 2021). If the heat demand for the DAC system is not fully fulfilled, the deficit is assumed to be supplied by adding flat-plate solar thermal collectors, given that global horizontal irradiation (GHI) would be high for the chosen location. Overall, solar heat fulfils the total auxiliary energy demand, directly and indirectly, to make the fuel plant energy self-sufficient, given its remote location. In the Near-term future, the power block output exceeds the auxiliary electrical energy demand due to the lower heat-to-syngas efficiency and higher waste heat, generating a surplus of electricity that was assumed to be exported out of the system.

2.3. Economic model

The fuel production cost is determined using the minimum fuel selling price (MFSP) method. The MFSP corresponds to the levelized cost of energy for fuels. This method establishes the minimum price for the fuel to recover the investment within a specified time frame, assumed 25 years. The MFSP is, therefore, the minimum selling price to have a net present value of at least zero over the assumed lifetime of the project. The formula of the MFSP can be found in Eq. (4).

$$MFSP = \frac{\sum_{t=0}^{Lifetime} \frac{C_t + IT_t + T_t + L_t + O_t + F_t - N_t}{(1+D)^t}}{\sum_{t=0}^{Lifetime} \frac{E_t}{(1+D)^t}} \qquad (4)$$

where:

- C_t is capital expenditure (CAPEX) in year t
- IT_t is the interest payment in year t
- T_t is the transport cost to Europe
- L_t is the labour cost
- O_t is the operational expenditures (OPEX) in year t
- F_t is the fixed costs i.e. local taxes, insurance, administrative and marketing costs
- N_t is the revenue from a potential surplus of electricity
- E_t is the annual production volume of fuel
- D is the discount rate.

Three MFSPs are calculated, i.e. MFSP of the plant if decided to be built in the near-term future (operations starting by 2030), the MFSP of the long-term future "Nth" plant built in the 2030s decade with baseline assumptions and the MFSP of the "Nth" plant built in the 2030s decade with optimistic assumptions. For the near-term future's plant, only one scenario is modelled. This scenario considers a technologically mature design of the technology modelled with the current cost of state-of-the-art components of this technology. The data for the long-term future baseline scenario differ from those used for the near-term future plant for all components where high technological learning is expected, e.g. DAC, redox reactor, solar field etc. The long-term baseline scenario represents average estimates from the literature for these components' future costs. Data for the optimistic scenario represent the most optimistic cost assumptions, which means the lowest achievable in the

2030s decade. The discount rate for established renewable technologies (hydropower, photovoltaics and onshore wind) is between 5 % and 8 % in Europe (Thornton, 2019). We assume a discount rate of 6.5 %, except for the optimistic scenario, where a 5 % discount rate is assumed. Appendix A presents further details of the financial assumptions (Table A.1).

With respect to CAPEX, several equipment installed costs commonly scale with the capacity. The scaling formula (Eq. (5)) is used to estimate the equipment cost with the technical model's fuel capacity output (q_t). A scaling factor (X) is needed to apply such a formula. X typically ranges between 0.6 and 0.7 for most chemical processing reactors, pumps, and other auxiliaries (Ereev and Patel, 2012). Modular pieces of equipment have a scaling factor close to 1.

$$CAPEX_t = CAPEX_0 \left(\frac{q_t}{q_0}\right)^X \qquad (5)$$

When averaging CAPEX data from different sources, the same scaling factor X is applied to make all values refer to a single reference capacity (q_0) from one source. Data are based on peer-reviewed and grey literature and own estimations when the source is not indicated.

We here highlight capital costs assumed for the major components of the solar fuel pathway. Appendix A presents further details on CAPEX for the syngas conversion to the different fuels and other OPEX/CAPEX assumptions.

Heliostat field – The heliostat field (including the tower) is assumed to cost 120 €/m² near-term future, 100 €/m² and 70 €/m² in the future, respectively, for baseline and optimistic scenarios. These assumptions align with other literature sources (DOE, 2021; Falter et al., 2016; Falter and Sizmann, 2022; Monnerie et al., 2020). The US department of energy (DOE) also estimates the cost of heliostat (excl. tower) to go below 70 €/m² for 2030 (DOE, 2021) and potentially as low as 50 €/m² (U.S. DoE, 2017). No scaling factor is assumed for the solar field. So, these cost data are assumed to be valid also for the modelled capacity.

Receiver – The current cost of a solar receiver for a plant of 1.08 km² is 60.9 M$ (Kurup et al., 2022). This means that the receiver adds an additional cost of about 50 €/m² to the solar system in the near-term future. Receiver costs (and tower costs) are expected to decrease by 10–30 % in 2030 (DOE, 2021). Accordingly, we assumed the receiver cost to contribute 35 (optimistic)-40 (baseline) €/m² in the long-term future.

Direct air capture – We assume near-term future's CAPEX of low-temperature adsorption DAC of 360 kt CO_2/year capacity to be 730 €/t CO_2*year (Fasihi et al., 2019). Within this cost, there are DAC construction costs, DAC's vacuum pumps, blowers and heat exchangers. This aligns with the lowest values of the range 800–900 $/t CO_2*year reported by other sources (Brilman, 2020). Starting from 730 €/t CO_2*year, Fasihi et al. provide two estimates of 2050 CAPEX costs of DAC plants with a reference capacity (q_0) of 360 kt/year: 199 €/t*year (high-cost) and 84 €/t*year (low-cost). These two estimates rely on projected global DAC installed capacities ($Q_{t=2050}$) in 2050 of 7679 and 15,357 Mt CO_2/year (Fasihi et al., 2019), respectively. We assume linear growth to these installed capacities starting from the 2020 value of 3 Mt CO_2/year (Becattini et al., 2021), which leads to 2035 values of 3840 and 7680 Mt CO_2/year. Based on the assumed 2050 installed capacity and costs, this is equivalent to a learning rate of 10 % in the baseline (Nth) scenario and 16 % in the optimistic (Nth) scenario. Accordingly, 2035 DAC CAPEX is assumed to be 237 €/t CO_2*year in the baseline scenario (i.e. 9 €/t CO_2) and 100 €/t CO_2*year in the optimistic scenario (i.e. 4 €/t CO_2). No scaling factor is considered for DAC. Therefore, the DAC capacity derived from the technical model does not affect the specific CAPEX of DAC. Sorbents, a major cost source for DAC (Bos et al., 2020; Holmes et al., 2021; Yu et al., 2017), are assumed not to be

included in the abovementioned DAC's CAPEX. Although sorbent costs are high, most studies have not considered them when calculating the cost of CO_2 from DAC (Brilman, 2020). The current Climeworks' DAC technology consumes 7.5 kg of sorbent per t of CO_2 captured (Deutz and Bardow, 2021). This figure is expected to decrease to 3 kg/t CO_2 in the future (Deutz and Bardow, 2021; Terlouw et al., 2021). Accordingly, we assume a sorbent consumption of 7.5 kg/t CO_2 for near-term future and 3 kg/t CO_2 for the long-term future (for both baseline and optimistic). The current cost of DAC sorbent ranges between 13 and 50 €/kg (Bos et al., 2020; Holmes et al., 2021; National Academies of Sciences, Engineering, 2019; Sinha and Realff, 2019; Wijesiri et al., 2019; Yu et al., 2017). On the other hand, multiplying DAC sorbents' raw material mass fractions (65%wt PEI and 35%wt silica) and raw material costs leads to only 1.2–2.6 €/kg (Leonzio et al., 2022; Wijesiri et al., 2019). We therefore assume 15 €/kg for near-term future (representing a low-priced sorbent) and 8 €/kg (baseline) and 2 €/kg (optimistic) for the long-term future. The solar field provides heat and energy for DAC (see Section 2.2). However, to picture our assumptions for CAPEX and sorbent with respect to the final CO_2 cost, if we assume 50 €/MWh for electricity and 25 €/MWh for heat, this would mean a DAC CO_2 cost of 280 €/t near-term future, 100 €/t for future baseline and 75 €/t for future optimistic. These values align with the future DAC cost between $86 and $221 per t CO_2 calculated by Sinha and Realff (2019). Compared with the first operating DAC plants, Climeworks estimated 2017 DAC cost of the 900-t/year Hinwil facility to be around 600 $/t (Brilman, 2020; Evans, 2017; Kramer, 2018). Climeworks aims to reach $200/t within 3–5 years (Evans, 2017; Kramer, 2018) and estimates that future plants could reduce this value to below 100 $/t, with a target for very large-scale plants of 75 $/t (Brilman, 2020). Hence, our values align also well with Climeworks' expectations.

Power block – The power block's CAPEX for the near-term future's scenario is based on a recent publication performing a cost analysis of liquid fuel production from H_2 and CO_2 (Zang et al., 2021). In their study, the power block of 16 MW net output is assumed to consist of a steam turbine, boiler and wastewater treatment for a total cost of 18.9 M€. For the same capacity, based on (DOE, 2021), future estimates lead to 14.4 M€ for the future baseline and 11.2 M€ for the future optimistic scenario. A scaling factor of 0.6 was assumed for the power block (Zang et al., 2021). Surplus electricity generated in the near-term future scenario is valued at 50 €/MWh.

Solar redox – Near-term future's redox reactor cost is taken from Falter et al. (2020): 126 M€ for a capacity of 35 kt H_2/year. This value is used for near-term future's scenario. Two-thirds of the cost is due to the reactive material (Falter et al., 2020). Using the H_2 molar flow to convert the costs of the technology when producing CO instead of H_2, the redox reactor to produce 35 kt CO/year costs 9 M€. The future optimistic estimate of 38 M€ for 35 kt H_2/year is taken from Onigbajumo et al. (2022), assuming no scaling effects from the size assumed in the source. The average value between Falter et al. (2020) and Onigbajumo et al. (2022) is assumed for the future baseline scenario, i.e. 82 M€ for 35 kt H_2/year. The redox reactor is accompanied by heat exchangers (HXs), whose near-term future cost is estimated to be 0.76 M€ for a production capacity of 100 t H_2/year (scaling factor 0.6). For the heat exchangers, the future optimistic value is taken from Onigbajumo et al. (2022): 0.11 M€ for 100 t H_2/year after considering the scaling effect. The future baseline value is assumed to be 0.44 M€ which reflects the average between the optimistic value and the value assumed for the near-term future, i.e. 0.76 M€ for 100 t H_2/year.

Vacuum pumps – Vacuum pumps remove evolving oxygen from the thermochemical reactors and their CAPEX depends strongly on the targeted pressure level. The reduction pressure maximizing the reactor energy conversion efficiency is 1000 Pa (Falter et al., 2020). The assumption of pump efficiencies is a common flaw in cost

Table 2

Background life cycle inventory data. The ecoinvent database was used as the near-term future's major source for life cycle inventory data. Future life cycle GHG emissions are mostly determined starting from the data assumed for the near-term future (see column "Future").

Component (production and supply of)	Near-term future	Long-term future
Heliostat field with tower	Collector field area, solar tower power plant, 20 MW {GLO}|market for collector field area, solar tower power plant, 20 MW|cut-off	Life cycle GHG emissions of the heliostat field were assumed to decrease linearly with steel production's GHG emissions, which are expected to drop between 7 % (baseline) and 14 % (optimistic) by 2050 (IEA, 2022).
Receiver	Receiver system, solar tower power plant, 20 MW {GLO}|market for receiver system, solar tower power plant, 20 MW|cut-off	Life cycle GHG emissions of the receiver were assumed to decrease linearly with steel production's GHG emissions, which are expected to drop between 7 % (baseline) and 14 % (optimistic) by 2050 (IEA, 2022).
Power block	Power block installation, solar tower power plant, 20 MW RoW|cut-off	Based on the dynamic LCA modelling by Reinert et al., power block life cycle GHG emissions are assumed to be 13 % lower by 2050 (Reinert et al., 2021). A linear decrease was assumed from near-term future's value to derive 2035 value.
TES material	Aluminium oxide, metallurgical {IAI Area, EU27 & EFTA}|aluminium oxide production|cut-off	Alumina: Aluminium oxide, metallurgical {IAI Area, EU27 & EFTA}|aluminium oxide production|Cut-off. Mullite: Refractory, fireclay, packed {DE}|production|cut-off.
Thermal storage system (excluding heat storage material)	Thermal storage system construction, solar tower power plant, 20 MW RoW|cut-off. The TES material was removed from the dataset.	As for near-term future.
DAC sorbents	4.8 kg CO_2eq/kg of sorbents (Deutz and Bardow, 2021)	3.3 kg CO_2eq/kg of sorbents (Deutz and Bardow, 2021)
DAC construction	14 g CO_2eq/kg CO_2 captured (Deutz and Bardow, 2021)	13 g CO_2eq/kg CO_2 captured (Deutz and Bardow, 2021)
Transport by train in Europe	Transport, freight train {RER}|market group for transport, freight train|cut-off	Assumed net zero by 2035
Transport by train outside Europe	Transport, freight train {RoW}|market for|cut-off	No variation compared to near-term future was assumed.
Transport by ship	Transport, freight, sea, tanker for petroleum {GLO}|market for transport, freight, sea, tanker for petroleum|cut-off	We assumed 13 % lower GHG emissions than near-term future based on the target of RED II revision: The FuelEU Maritime proposal
Ceria	Cerium oxide {GLO}|market for cerium oxide|cut-off.	As for near-term future.

Table 2 (*continued*)

Component (production and supply of)	Near-term future	Long-term future
Monoethanolamine (MEA)	Ceria mass loading not disclosed. Monoethanolamine {RER}| ethanolamine production| cut-off	As for near-term future.
Flat plate solar collector	Flat plate solar collector, Cu absorber {GLO}|market for| cut-off	Life cycle GHG emissions of the flat plate solar collector were assumed to decrease linearly with steel production's GHG emissions, which are expected to drop between 7 % (baseline) and 14 % (optimistic) by 2050 (IEA, 2022).

estimates for vacuum pumps that lower the oxygen partial pressure in solar redox reactors (Brendelberger et al., 2017). We retrieve the vacuum pump's baseline cost from an analysis of vacuum pump performances used in large-scale industrial applications in the context of the targeted redox cycles. According to such a study (Brendelberger et al., 2017), vacuum pumps operating at 1000 Pa cost between 0.10 M€ and 0.15 M€ per molar flow of oxygen (mol/s) (Brendelberger et al., 2017). The average value between these two means 0.43 M€ per 100 t of H_2/year split from water (and 0.03 M€ per 100 t of CO split from CO_2, based on molar mass ratios). A more

optimistic source was used for the long-term future optimistic scenario, converting the value assuming a scaling factor of 0.65 (Onigbajumo et al., 2022), leading to 0.34 M€ per 100 t of H_2/year and 0.02 M€ per 100 t of CO/year.

Thermal energy storage – The technical model calculates the required capacity in MWh of the intra-day TES system and needs to be translated into the volume of thermal storage filler material, i.e. alumina or mullite. In particular, mullite use is under investigation as an alternative material to alumina, potentially resulting in further cost reduction. Besides being more expensive, alumina might also be too brittle. For the economic model, we assume alumina for the near-term future and the long-term future baseline scenarios and mullite for the long-term future optimistic scenario. An alumina-based TES of capacity $q_0 = 108$ m^3 (in line with 100 t/year H_2) has a near-term future CAPEX of 1.85 M€. With alumina's density of 3990 kg/m^3 (Marur et al., 2004), a heat capacity of 132 kJ/kg (at 1500 °C with heat exchange operating with a ΔT of 100 °C) and void fraction of 37 %, the alumina mass is 271 t for the specified volume. For the same thermal capacity, the mullite mass is 379 t, based on mullite's heat capacity of 129 kJ/kg (at 1500 °C with heat exchange operating with a ΔT of 100 °C). The corresponding volume of the mullite-based TES is 137 m^3, calculated considering its density of 3200 kg/m^3 (Mishra and Ningthoujam, 2017) and void fraction of 57 %. Using the reference capacity q_0 of 5415 m^3 and reference CAPEX$_0$ of 16.05 M€, the mullite-based TES volume of 137 m^3 (corresponding to a production of 100 t/year H_2) has a CAPEX of 1.22 M€, showing that mullite-based TES is a cheaper solution compared to alumina-based TES. The same assumptions are also used for the buffer TES, which
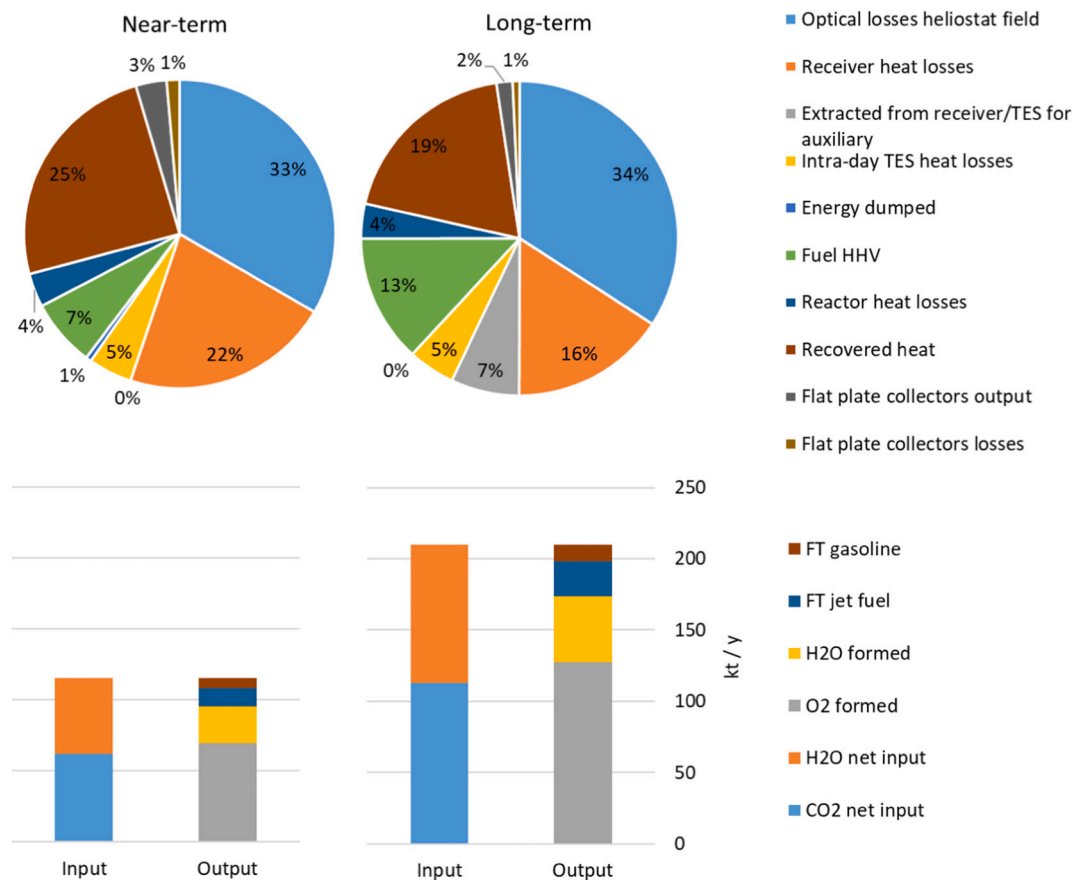

Fig. 2. Case: Sierra Gorda (Chile), FT jet fuel. On the left, near-term future scenario. On the right, long-term future scenario. On top, energy balance of the solar fuel production plant as a percentage of total DNI incident on heliostat field and GHI on flat plate collectors. Bottom, mass balance. "H_2O formed" refers to water formed in the FT synthesis, which is assumed to be recycled back into the process. "H_2O net input" refers to net water input required by the process after recycling unreacted H_2O from redox reactor products and water formed in the FT synthesis.

has a smaller volume than the intra-day TES based on the technical model outcome (see Table 3). Hence, a different assumption for the buffer TES would have a negligible effect on the calculated fuel cost. A scaling factor of 0.7 is applied for TES.

2.4. Environmental sustainability model

The environmental sustainability model contains a life cycle assessment (LCA) evaluation aiming to assess the potential of solar fuels to be considered sustainable in the current and future European market. This involves calculating the life cycle GHG emissions with respective environmental hotspots over the supply chain. LCA methodology is standardized by ISO 14040 and ISO 14044 (ISO, 2006a, ISO, 2006b). The well-to-wheel methodology (WTW) is a sub-category of the LCA methodology adopted for the EU alternative fuel policy decision context (EU, 2015; European Commission, 2016). The WTW methodology focuses on feedstock production, feedstock conversion into fuel, transportation, and fuel combustion. All components included in our WTW assessment can be found in Table 2, with respective background data extracted from the ecoinvent 3.8 database (Ecoinvent, 2022).

The EU measures the sustainability of alternative fuels in terms of WTW GHG emissions reduction per GJ of lower heating value (LHV). Accordingly, the functional unit of 1 GJ of fuel is adopted in this study. The reduction is calculated as the difference between the WTW GHG emissions of the alternative fuel and a default value for fossil fuels, i.e. the so-called EU fossil fuel comparator (EU, 2015; European Commission, 2016). According to EU RED II (EC, 2018), the fossil fuel comparator is 94 kg CO_2eq/GJ for liquid fuels and 80 kg CO_2eq/GJ for gaseous fuels. Any blending limit is neglected in the emissions reduction calculation and the CO_2 combustion emissions of the alternative fuel are considered carbon neutral (EU, 2015; European Commission, 2016). We calculate WTW GHG emissions and GHG emissions savings compared to conventional fuels for both the near-term future and the long-term future. Energy allocation is used to account for the potential electricity surplus generated together with the fuels in the near-term future scenario. For fuels, as recommended by the EU RED II (EC, 2018), the lower heating value was used to allocate the environmental impacts between co-products. The following components were subject to the allocation procedure between fuels and electricity surplus: heliostat field with tower, receiver, power block and TES.

3. Results

3.1. Energy and mass balance

3.1.1. Sierra Gorda

Fig. 2 plots the energy and mass balance of the solar fuel production plant calculated by the technical model for the case Sierra Gorda (Chile) for the production of FT jet fuel. Major energy losses include optical losses in the heliostat field and heat losses from the receiver. The fuel's HHV is the total of the two fuels produced in this case, FT jet fuel and FT gasoline. It also represents the overall solar-to-fuel efficiency as a percentage, defined as the ratio of the fuel HHV to the total DNI incident on the heliostat field and GHI incident on the flat plate collectors, if applicable. A solar-to-fuel efficiency of 13 % is obtained for the Long-term future case, given the optimistic efficiency assumptions, while 7 % is obtained for the Near-term future case, owing to the conservative receiver and redox reactor efficiencies and higher auxiliary energy demand from the DAC system. The recovered heat portion represents the unutilized thermal energy recovered from the reactor, which is utilized for meeting auxiliary energy demand. Thus, for Sierra Gorda, with an annual total DNI of 3468 kW/m^2, a heliostat field size of 1 km^2, and optimistic technical assumptions (Long-term future), the plant produces an annual total output of 24.3 kt of FT jet fuel and 12.1 kt of co-produced FT gasoline. Besides oxygen produced during the reduction step, a significant quantity of water is also produced during fuel synthesis, which

Table 3

Calculated capacities for an FT fuel production plant relying on a 1 km^2 solar field for each location for the near-term future and long-term future. Heliostat field of 1 km^2 (3 km^2 land area). If jet fuel production is targeted, the share of jet fuel in the mix is 67%wt. If diesel production is targeted, the diesel share in the FT fuel mix is 79 %.

Calculated capacity	Sierra Gorda, Chile		Tabernas, Spain		Ouarzazate, Morocco	
	Near-term future	Long-term future	Near-term future	Long-term future	Near-term future	Long-term future
Annual total DNI (kWh/ m^2/year)	3468	3468	2234	2234	2601	2601
Annual solar-to-fuel (HHV) efficiency (%)	7.1	13.2	6.7	13.0	7.0	13.1
FT fuels output (kt/year)	20.0	36.4	12.2	23.2	14.8	27.2
DAC (kt CO_2/ year)	61.9	113.0	37.7	71.8	46.0	84.4
H$_2$ output solar redox (kt H$_2$/ year)	6.0	10.9	3.6	6.9	4.4	8.1
CO output from solar redox (kt CO/year)	39.4	71.9	24.0	45.7	29.3	53.7
Powerblock steam turbine (MW$_e$)	29	20	20	14	23	15
Flat plate collectors (km^2)	0.04	0.02	0.03	0.02	0.03	0.02
Thermal capacity intra-day TES (MW$_{th}$)	4392	2860	2996	4131	3357	2703
Thermal capacity buffer TES (MW$_{th}$)	74	50	50	34	56	38
Electricity surplus (MWh$_e$/year)	137,941	51	84,058	32	102,386	38
Electricity (% energy over total energy output made of electricity + LHV of fuels)	37 %	0 %	37 %	0 %	37 %	0 %

is recycled back to the gross water input. Overall, the technical analysis indicates that the solar thermochemical pathway could produce fuel at relatively high solar-to-fuel efficiencies while fully fulfilling its auxiliary energy requirements using recovered heat.

3.1.2. Effect of location

Table 3 compares the components' size and overall efficiencies among different locations and between the near-term and long-term future for the production of FT fuels. The plant's location in relation to the DNI significantly impacts the annual fuel production, considering the fixed size of the solar field. As a result, the solar-to-fuel efficiency will increase if the annual DNI of the location increases. In the short term, the solar-to-fuel conversion efficiency is relatively low, leading to a reduced output of fuels. Consequently, more solar energy is converted into electricity, surpassing the fuel plant's electricity requirements, leading to a substantial electricity surplus that can be exported. The electricity surplus is about 37 % of the total energy output of the plant in the near-term future scenario, while it is negligible in the long-term future scenario. The same trend is observed for the other fuel routes, i. e. solar thermochemical fuels via methanol synthesis and hydrogen
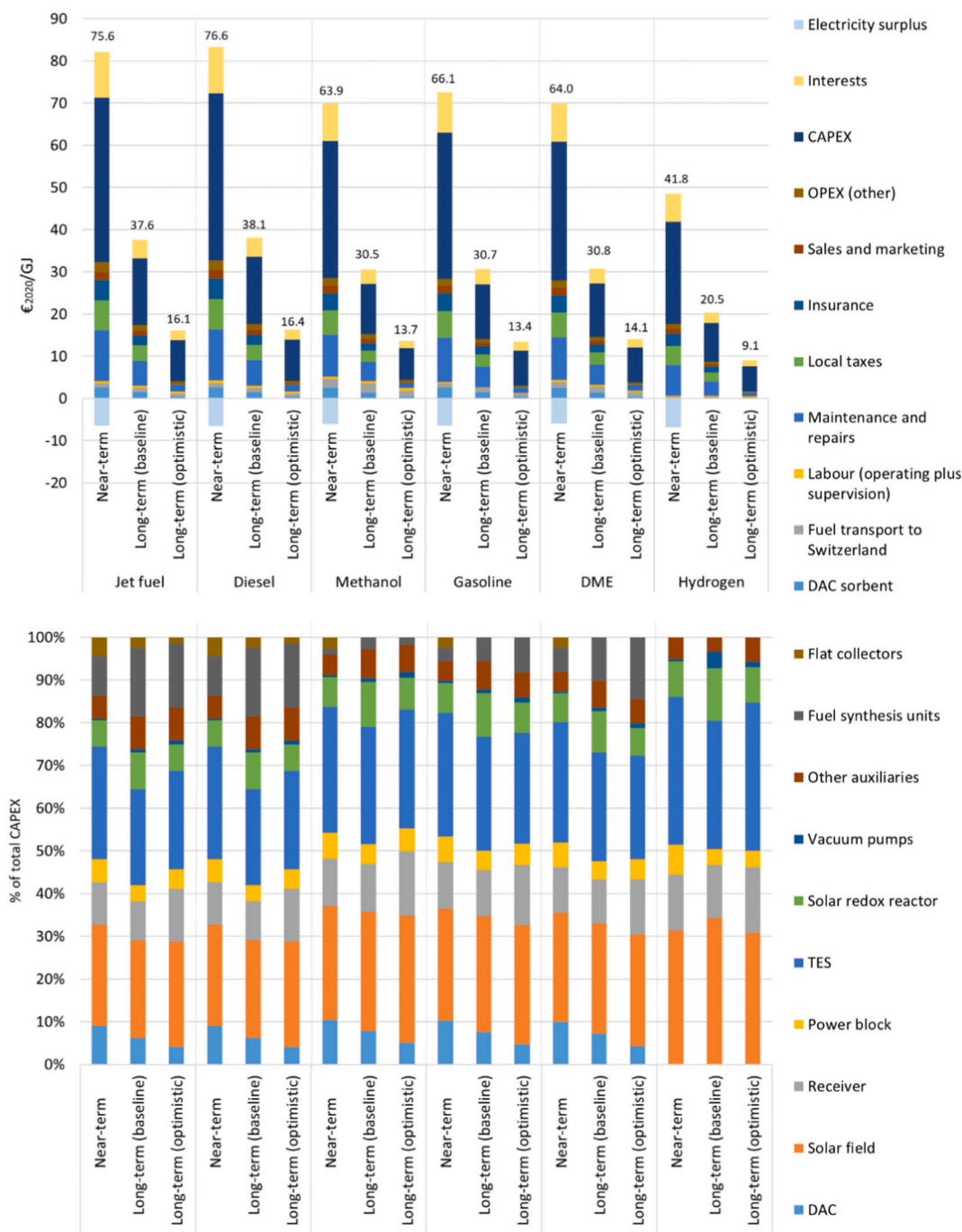
Fig. 3. Minimum fuel selling price ($€_{2020}$) with cost-built up for one GJ of fuel produced via the solar thermochemical pathway in Sierra Gorda. 25 years lifetime. See Appendix B for numerical values (Table B.3). The breakdown of CAPEX for each fuel and scenario is provided in the bottom graph. Note: hydrogen transportation does not include hydrogen liquefaction.

production (see Appendix B, table B.1 for methanol and table B.2 for hydrogen).

3.2. Minimum fuel selling price

3.2.1. Sierra Gorda

Fig. 3 shows the MFSP with its breakdown of each investigated fuel if produced in Sierra Gorda (Chile), i.e. the location with the highest DNI among the three selected locations. See Section 3.2.2 for the effect of the location on MFSPs.

3.2.1.1. Near-term future.
Per unit of energy content (LHV), jet fuel and

diesel produced via FT process by a plant built in the near-term future have both MFSPs of 75.6 €/GJ (i.e. about 2.5 €/L). CAPEX represents about half of the total MFSP (39.1 €/GJ). The main cost contributions to the CAPEX of FT fuels are the following: the solar field (~9.3 €/GJ), TES (~10.3 €/GJ), DAC (~3.5 €/GJ), fuel synthesis (~3.7 €/GJ) and receiver (~3.9 €/GJ). Both assumed to be proportional to CAPEX, maintenance and local taxes contribute to about 11.9 €/GJ and 7 €/GJ, respectively. Other major cost sources are interests (~10.7 €/GJ) and DAC sorbents (~2.6 €/GJ). Gasoline via methanol, methanol, and DME showed an MFSP up to 15 % lower than FT jet fuel and diesel, ranging between 63 and 66 €/GJ in the near-term future.

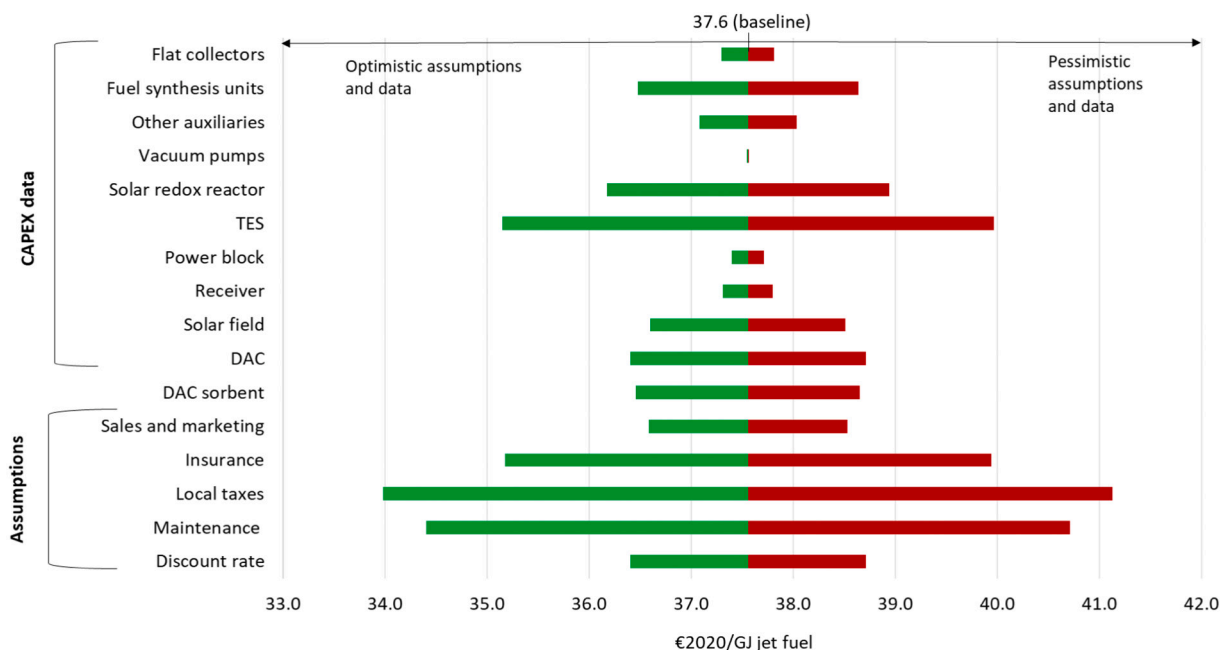On a volume basis, such figures translate into an MFSP of 2.5 €/L for

Fig. 4. Sensitivity analysis illustrating the effect on long-term future minimum fuel selling price (€₂₀₂₀) of FT jet fuel by varying economic data and assumptions one by one from baseline (based on average estimates from the literature for each component's cost) to the optimistic scenario (based on the most optimistic estimates from the literature for each component's cost). See Section 2.3 for exact values. Pessimistic figures refer symmetrically to the opposite trend.

jet fuel and diesel, 2.2 €/L for gasoline via methanol, 1.0 €/L for methanol and 1.2 €/L for DME. To compare, jet fuel price is around 0.5–0.9 €/L (IATA, 2022), the price of gasoline and diesel without taxes is around 0.7–0.9 €/L (EC, 2023), methanol price around 0.3–0.45 €/L (Methanex, 2023) and DME price around 0.35 €/L (Skorikova et al., 2020). The CAPEX per unit of energy for fuel synthesis is significantly lower for methanol than for FT synthesis. Hence, the less technically challenging methanol synthesis is more cost-effective than multiple-step Fischer-Tropsch synthesis, also considering that methanol synthesis can be operated at lower temperatures and pressures, reducing reactors' capital costs. However, Fischer-Tropsch synthesis produces a wider range of hydrocarbons (including jet fuel) with higher market value than methanol (Tsongidis et al., 2019).

Per unit of energy, hydrogen via solar thermochemical pathways with a cost of 41.8 €/GJ is much cheaper than other fuels in the near-term future. This technology can produce hydrogen from water with no need for further refining (and therefore no need for fuel synthesis units), resulting in the highest solar-to-fuel (LHV) efficiency (almost 10 %). Furthermore, no DAC is needed for hydrogen production. However, hydrogen transportation via shipping requires further costly processing, e.g. liquefaction (not considered in our analysis), adding a further cost estimated in the order of 6–7 €/GJ (Kim et al., 2021).

3.2.1.2. Long-term future. Future MFSPs vary significantly between baseline and optimistic scenarios. Jet fuel and diesel via FT process have both an MFSP of 16.1–37.6 €/GJ, methanol of 13.7–30.5 €/GJ, gasoline of 13.4–30.7 €/GJ, DME of 14.1–30.8 €/GJ and hydrogen of 9.1–20.5 €/G.J. Hence, we estimate MFSPs to decrease by 50 % to 80 % in the future compared to near-term future. These variations have a multitude of sources. To highlight the key factors, Fig. 4 presents the sensitivity analysis results for the long-term MFSP of FT jet fuel (baseline) with each assumption and data point varied from average (baseline) to the most optimistic. This analysis allows us to identify the most critical variables in the economic model and their impact on the MFSP. Baseline MFSP relied on average input cost data and assumptions i.e. the average cost data in a range going from optimistic to pessimistic. Fig. 4 shows also how a potential pessimistic trend in a single variable can impact the total cost, e.g. due to a component's future cost decreasing less than

expected on average.

The sensitivity analysis shows that (pure) assumptions and data uncertainty cause the main differences in the MFSP between the two scenarios. All OPEX assumptions have a high impact on the MFSP. Due to a single one of these OPEX assumptions, the MFSP can vary up to 4 €/GJ. The most impactful OPEX assumptions are the following ones ranked by weight: first, reducing maintenance and repair costs from 2.5 % of CAPEX per year to 1 % of CAPEX per year; second, eliminating local taxes, e.g. assuming state-supported tax exemptions, which stand at 1.5 % of CAPEX per year in the baseline scenario; third, removing the allocation of insurance costs to such fuels, currently set at 1 % of CAPEX per year in the baseline scenario; and fourth, decreasing sales and marketing expenses from 6.5 % of OPEX to 2 % of OPEX. By changing these assumptions, we can impact overall OPEX performance the most. Concerning financial assumptions, varying the discount rate from 6.5 % to 5 % changes the MFSP by 1.2 €/GJ.

The variation in CAPEX of the solar field and TES can vary the MFSP by about 1.0 €/GJ and 2.5 €/GJ, respectively. CAPEX for DAC, fuel synthesis units, and the solar redox reactor can vary the MFSP by up to 1.5 €/GJ. See Section 2.3 for CAPEX data used for DAC and the solar redox reactor for all scenarios. In the case of fuel synthesis, the optimistic case assumes to have co-location with a refinery where FT's intermediate product "syncrude" is upgraded to the final fuels. If co-located with a shared refinery, FT synthesis CAPEX can be reduced by 40 % compared to a stand-alone plant (Jones et al., 2009). DAC sorbents cost variations have a similar effect (on the order of 1.1 €/GJ).

3.2.2. Effect of location
Fig. 5 shows the effect of the location on the MFSP of jet fuel, taken as a representative case to discuss the general trend also observed for other fuels.

The distance of a location from Europe (Switzerland) has a minor impact on the cost of producing jet fuel. The main factor affecting cost is the variation in CAPEX, with Spain and Morocco experiencing a 23–33 % higher MFSP of jet fuel than Chile. The difference in CAPEX is primarily due to the lower DNI in Spain and Morocco, which leads to less fuel produced per m² of solar fields (and number of receivers) and therefore per MWₜₕ TES capacity (see Table 3). In the near-term future
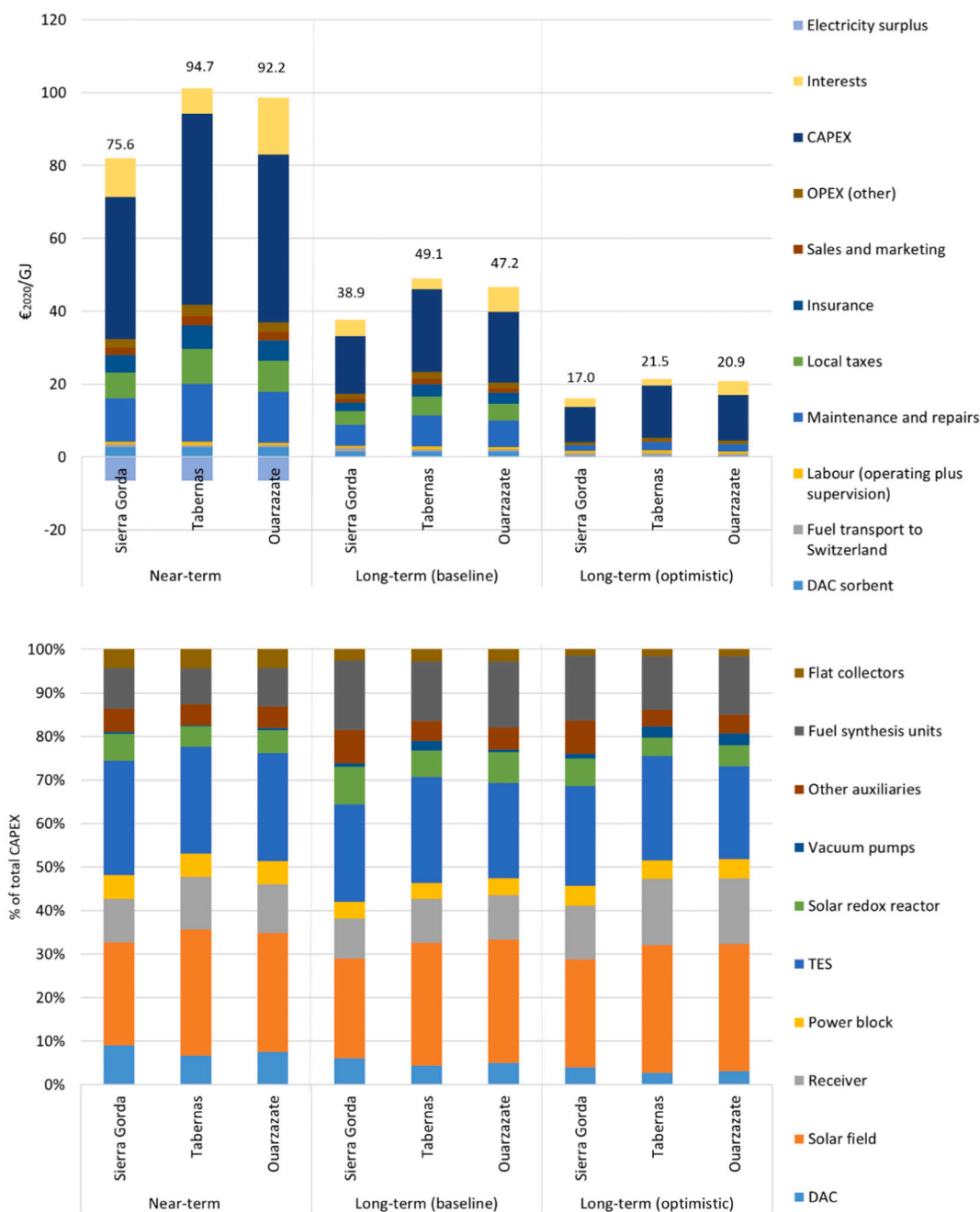
Fig. 5. Effect of the location on the minimum fuel selling price ($€_{2020}$) with cost-built up for one GJ of jet fuel produced via the solar thermochemical pathway. 25 years lifetime. See Appendix for numerical values (Table B.3). CAPEX breakdown for each location and scenario is in the bottom graph.

scenario, the solar field cost alone represents 15.3 €/GJ for jet fuel in Spain and 12.5 €/GJ in Morocco, compared to only 9.3 €/GJ in Chile. Additionally, the receiver accounts for 6.4 €/GJ of jet fuel's MFSP in Spain, and 5.2 €/GJ in Morocco, while it is only 3.9 €/GJ in Chile. Similarly, TES contributes for 12.9 €/GJ of jet fuel's MFSP in Spain, 11.5 €/GJ in Morocco, and only 10.3 €/GJ in Chile. Although Spain has a 14 % higher CAPEX contribution than Morocco, the difference in MFSP between the two is insignificant due to a more favourable interest rate in Spain than in Morocco (2.2 % versus 5.7 %). These trends (see Fig. 5) also remain in long-term future scenarios (both baseline and optimistic). However, it is essential to note that the initial investment cost for a plant with a fixed area of solar field is higher in sites with higher DNI. This is because such sites can produce more fuels per km^2. In absolute terms, for an industrial-scale fuel production plant relying on a 1 km^2 solar field,

the required investment is at least 500 M€ in Chile, 450 M€ in Morocco, and 415 M€ in Spain for the near-term future. These figures have the potential to decrease to as low as 285 M€ in Chile, 260 M€ in Morocco, and 270 M€ in Spain for a plant built in the long-term future, assuming the most optimistic scenario.
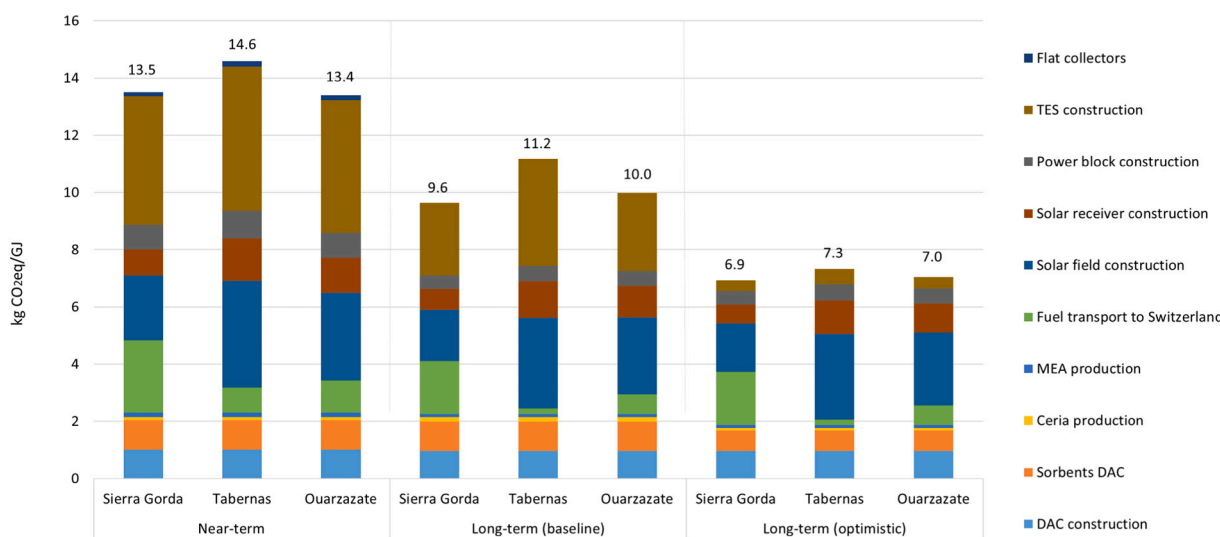
3.3. Life cycle GHG emissions

3.3.1. Sierra Gorda

Fig. 6 shows the life cycle GHG emissions with their breakdown of each investigated fuel if produced in Sierra Gorda (Chile), i.e. the location with the highest DNI among the three selected locations. See Section 3.3.2 for the effect of the location on life cycle GHG emissions.

Jet fuel, gasoline, diesel and DME show a similar trend among the
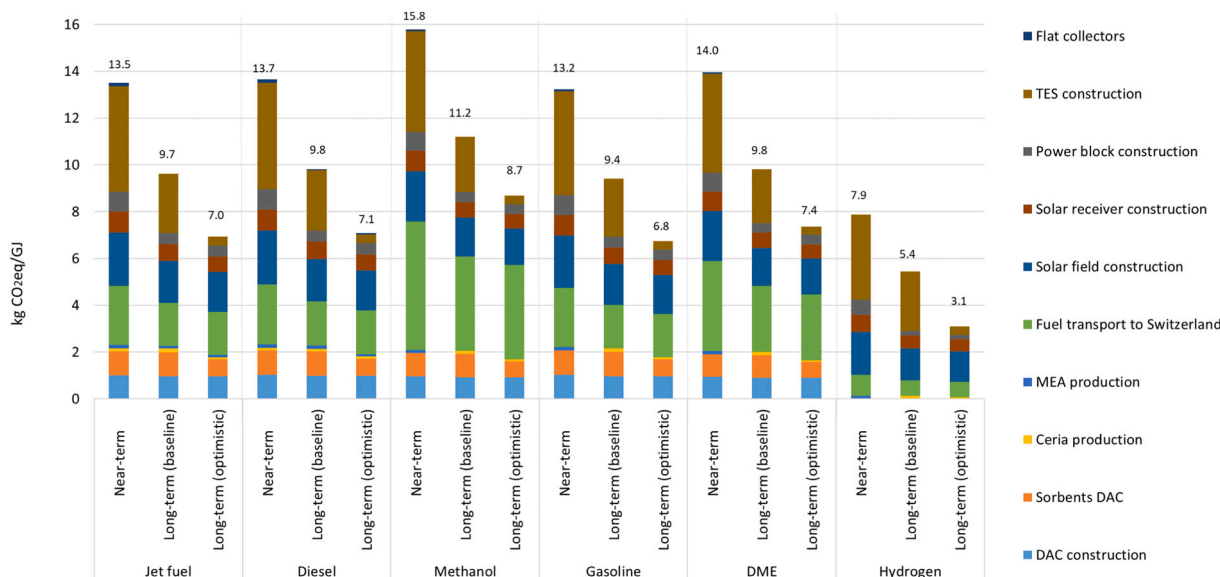
Fig. 6. Life cycle GHG emissions (kg CO_2eq/GJ) with the breakdown per GJ of fuel produced via the solar thermochemical pathway in Sierra Gorda. Numerical values can be found in Table B.6. The figure includes GHG emissions from parts replacements (i.e. ceria and DAC sorbents for this technology) commonly not accounted in GHG well-to-wheel methodology used to certify fuels' sustainability according to EU Renewable Energy Directive (JRC, CONCAWE, EUCAR, 2014). Note: hydrogen transportation does not include hydrogen liquefaction.

Fig. 7. Effect of the location on Life cycle GHG emissions (kg CO_2eq/GJ) with breakdown per GJ of fuel produced via the solar thermochemical pathway. See Appendix B for numerical values (table B.7). EU fossil fuel comparator: 94 kg CO_2/GJ (EC, 2018).

three scenarios. Near-term future's carbon footprint for these fuels is between 13.2 and 14.0 kg CO_2eq/GJ, the long-term future baseline between 9.4 and 9.8 kg CO_2eq/GJ and the long-term future optimistic between 6.8 and 7.4 kg CO_2eq/GJ. Methanol has a 15–20 % higher carbon footprint than these fuels due to the higher impact of transportation. The reason is that transportation is an important source of GHGs and is proportional to the mass to be transported, and methanol has a lower LHV than the other fuels considered. By contrast, hydrogen has a much lower carbon footprint per unit of energy than the other fuels, with a trend consistent with that of the MFSP. The high energy content of hydrogen also favours this. However, we remark that we neglected hydrogen compression or liquefaction needed for shipping. Hydrogen liquefaction alone adds 10–45 kg CO_2eq/GJ depending on the source of energy used in the process (Frank et al., 2021; Kim et al., 2021). The only relevant change in life cycle GHG emissions between long-term future baseline and long-term future optimistic scenarios is

due to the change in TES material (i.e. no more alumina but mullite).

For all fuels, compared to the reference values of the EU fossil fuel comparators, GHG savings are at least 80 % already in the near-term future. Given the low well-to-wheel GHG emissions, fuel transport to Switzerland is an important source of GHGs. However, a book-and-claim model could reduce such a GHG source, decoupling the sustainability claim from where that resource is physically consumed (SkyNRG, 2023). After 2050, GHG emissions will move further towards zero when all construction materials (e.g. steel, glass) are also manufactured using renewable energy.

3.3.2. Effect of location
Fig. 7 shows the effect of the location on the life cycle GHG emissions of jet fuel.
Fig. 7 shows a clear trade-off between the DNI's effect on the solar field and TES's environmental impact (linked to their size per unit of
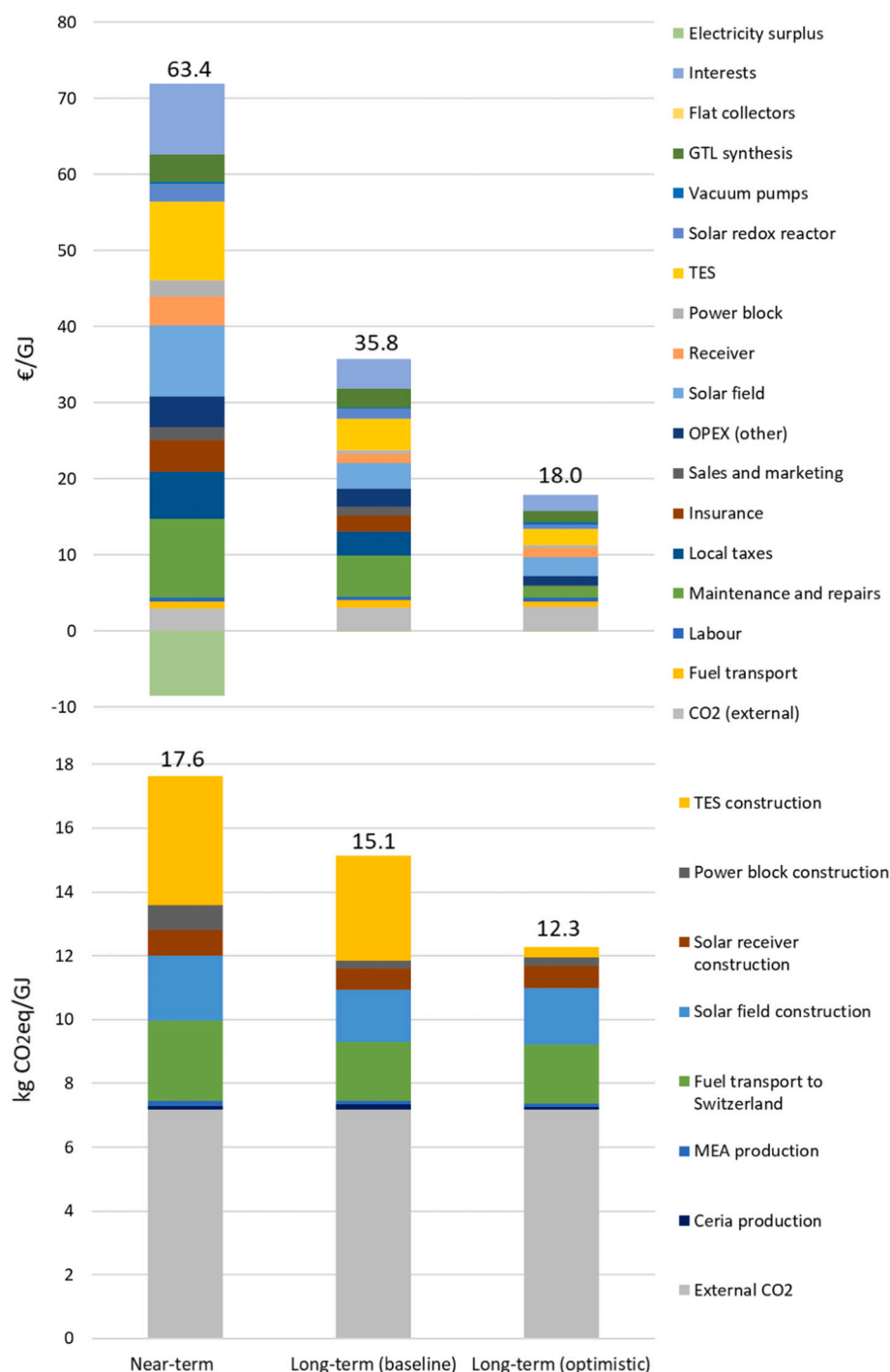
Fig. 8. Minimum fuel selling price ($€_{2020}$) with cost-built up and life cycle GHGs per GJ of jet fuel produced via the solar thermochemical pathway if relying on CO_2 from point source instead of air. External CO_2 is assumed to cost 50 €/t and have a carbon footprint of 0.1 kg CO_2eq/kg CO_2, reflecting, for example, cement plant CO_2. See Appendix B for numerical values (Table B.4). Note: the decrease in carbon footprint caused by TES construction is due to a different material assumed in the optimistic case.

fuel) and fuel transport to Switzerland (linked to the distance). However, the difference in life cycle GHG emissions is limited and does not impact the EU sustainability requirement of at least 70 % GHG savings compared to the fossil fuel comparator. Hence, based on life cycle GHG emissions, both a high DNI location far from Europe and a closer location with a relatively lower DNI are suitable for producing fuels from sun and air. However, as shown in Section 3.2.2, the location can have a much more important impact on fuel production costs.

4. Discussion

4.1. Change in CO_2 source

Capturing CO_2 from point sources is currently more cost-effective than capturing it directly from the air. The cost of capturing CO_2 from point sources varies significantly depending on the source's CO_2 concentration and the capture technology used (such as absorption versus adsorption). The capture costs typically range between 35 and 80 €/t (Dieterich et al., 2020; Moretti, 2023; Tsongidis et al., 2019). CO_2 from ethanol plants is the cheapest, followed by cement, and steel plants, while capturing CO_2 from gas-fired power plants is more expensive (Dieterich et al., 2020; Moretti, 2023). When considering most available
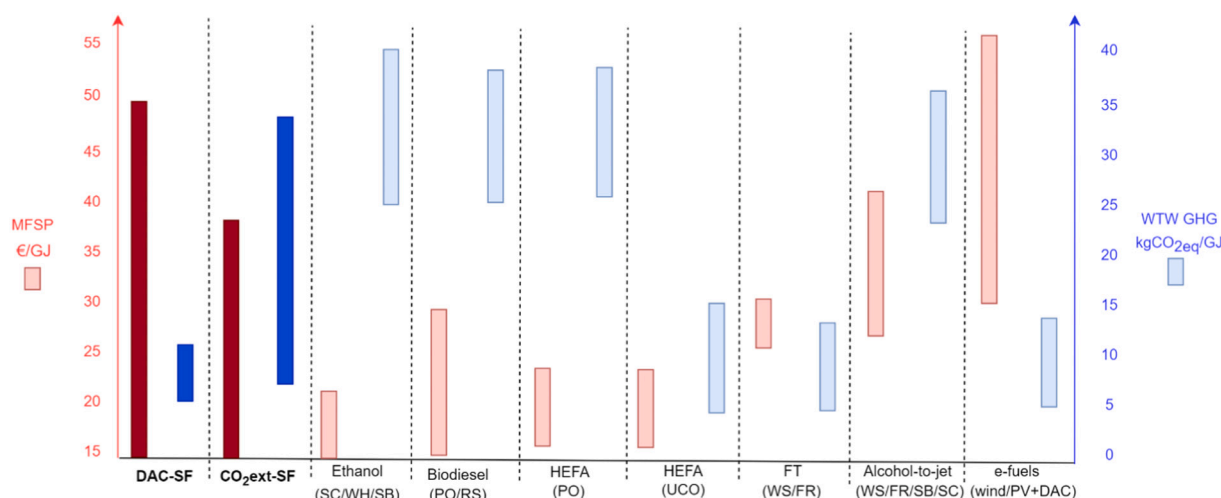
Fig. 9. Minimum fuel selling price and life cycle GHGs per GJ of fuel (long-term future, all three locations considered). Comparing the solar fuels (SF) produced via thermochemical pathway with biofuels and e-fuels. CO_2ext = CO_2 from concentrated point sources, SC = sugar cane, WH = wheat, SB = sugar beet, PO = palm oil, RS = rape seed, UCO = used cooking oil, WS = wheat straw, FR = forestry residues, PV = photovoltaic, HEFA = hydroprocessed esters and fatty acids. Costs and emissions for biofuels from Brown et al. (2020), Edwards et al. (2017), and Moretti et al. (2021) and for e-fuels from Concawe (2022).

carbon feedstocks, most have a carbon footprint of 0.02 to 0.3 kg CO_2eq/kg CO_2 (Moretti, 2023). These values are calculated using the current life cycle methodology for CO_2 feedstocks adopted by the EU Renewable Energy Directive II (EU, 2023). The carbon footprint calculated using the methodology recommended by such an EU directive does not distinguish strictly between biogenic and fossil sources. Still, it depends on the carbon footprint of energy and chemicals used for the capture process and the efficiency of the capture process. Once these factors are considered, the carbon footprint of the carbon feedstock is commonly the highest for fossil point sources and the lowest for CO_2 from ethanol fermentation plants, incineration plants and pulp mills (Moretti, 2023). Fig. 8 shows the MFSP and life cycle GHG emissions if jet fuel is produced using CO_2 from a point source.

On the one hand, the change of CO_2 source from air to point source can reduce costs, especially in near-term future's scenario. For example, a CO_2 source at 50 €/t could lead to an MFSP of 63.4 €/GJ in the near-term future (i.e. 2.1 €/L) and 18.0–35.8 €/GJ (i.e. 2.1 €/L) in the near-term future. These values align with Tsongidis et al., who analyzed solar fuels from point sources using a $NiFe_2O_4/NiFe_2O_{4-\delta}$ redox system produced in Greece. According to their study, FT fuels would yield a net profit of 0 when sold at a price of 0.206–0.567 €/kg combined with a feed-in-tariff of 0.0913–0.1125 €/kWh (Tsongidis et al., 2019), resulting in a total of 30.1–44.4 €/GJ once combined.

On the other hand, using CO_2 from a point source would increase the carbon footprint of the fuels compared to using CO_2 from DAC. However, the life cycle GHGs of any fuel produced via this pathway relying on CO_2 from point sources with a carbon footprint lower than 0.2 kg CO_2eq/kg CO_2 would still be considered sustainable in EU legislation terms (>70 % GHG savings). For example, suppose CO_2 is captured from a cement plant with a carbon footprint of 0.1 kg CO_2eq/kg CO_2 (Moretti, 2023) as in Fig. 8. In that case, the life cycle GHG emissions of jet fuel produced in Chile is between 12 and 18 kg CO_2eq/GJ (see Fig. 8), i.e. far below the maximum 28.2 kg CO_2eq/GJ allowed by EU Renewable Energy Directive II.

It is important to note that the EU adopted the delegated regulation C (2023)1086 in February 2023 (EU, 2023), which stipulates that emissions from the combustion of non-sustainable fuels used to generate electricity will only be considered avoided emissions until 2035. Similarly, emissions from non-sustainable fuels used in industries that are difficult to decarbonize will only be considered avoided emissions until 2040 (EU, 2023). This means that while CO_2 from fossil fuels can be used temporarily to produce solar fuels and benefit from EU incentives, their

production should shift to DAC or biogenic sources after the specified deadlines. Summarizing, a concentrated (fossil) CO_2 source instead of direct air capture can reduce near-future solar fuels' production costs favouring their initial scaling and, simultaneously, help achieve short-medium term GHG reduction targets. However, in the long term, only biogenic sources or DAC can supply CO_2 to such a technology to achieve carbon neutrality.

4.2. Benchmarking with other renewable fuels

Fig. 9 compares MFSPs and life cycle GHGs between the fuel produced via the solar thermochemical pathway, most common and future biofuels and e-fuels.

In locations with high DNI, the long-term future cost of fuels from sunlight and air lie in the range of 14 to 49 €/GJ (with the first plant between 48 and 70 €/GJ). This cost is in line with 17–44 €/GJ for advanced biofuels from bio-based by-products and wastes and slightly more expensive than 13–29 €/GJ for current biofuels from cultivated biomass feedstocks. At the same time, the future cost could be lower than e-fuels produced using hydrogen via electrolysis powered by renewables. For reference, the current price of fossil fuels is 8–14 €/GJ (Brown et al., 2020) with a production cost of 7–8 €/GJ (Concawe, 2022).

From a life cycle GHG perspective, fuels produced via the solar thermochemical pathway have far better environmental performance than most biofuels. Their life cycle GHGs align with advanced biofuels from wheat straw and forestry residues and future e-fuels from CO_2 and hydrogen produced via electrolysis powered with photovoltaic or wind. In particular, assuming 7–8 €/GJ for fossil fuels leads to costs per t of CO_2 avoided of fuels from sunlight and air of 700–850 €/t in the near-term future and 75–350 €/t in the long-term future. To contextualise, the GHG abatement costs for biofuels are around 40–510 €/t (Concawe, 2022). The GHG abatement costs for e-fuels are expected to be 460–1170 €/t in the short term and to reach 380–820 €/t in the long-term (Concawe, 2022).

5. Conclusions

This study demonstrates that solar thermochemical production of drop-in fuels in locations with high direct normal irradiation can become cost-competitive versus e-fuels using PV/wind electricity. In terms of GHGs emissions, the LCA of the two pathways give comparable

ranges. On the other hand, biofuels are on average less expensive but ultimately limited in the long-term scalability because of their limited feedstock and need to contain land use changes. Technical analysis indicates that an industrial-scale plant could achieve an overall solar-to-fuel energy efficiency of about 13–19 %, depending on the target fuel, in the long-term future with advancements in solar receiver, redox reactor, high-temperature heat recovery and direct air capture technologies.

Additionally, the life cycle assessment shows that greenhouse gas savings are already above the EU Renewable Energy Directive II requirement of 70 % for all fuels (relative to fossil fuels) and locations considered, with savings of over 80 % already achievable in the near-term future.

Furthermore, the study shows that using a concentrated CO_2 source from hard-to-abate industries like steel and cement plants instead of direct air capture for the first solar fuel plants can reduce near-term future costs while still meeting the EU Renewable Energy Directive II GHG reduction requirement.

The results demonstrate the potential of drop-in transportation fuels from sunlight and air to become a viable option in the future.

CRediT authorship contribution statement

Christian Moretti: Conceptualization, Methodology, Investigation, Data analysis, Visualization, Writing-Original draft, Project administration; **Vikas Patil:** Conceptualization, Methodology, Investigation, Data analysis, Visualization, Writing-Original draft, Data analysis, Visualization, Project administration; **Christoph Falter:** Methodology, Writing-Review & editing, Data analysis; **Lukas Geissbühler:** Writing-Review & editing, Data analysis; **Anthony Patt:** Conceptualization, Writing-Review & editing, Project administration, Funding acquisition, Supervision, Validation; **Aldo Steinfeld:** Conceptualization, Writing-Review & editing, Project Administration, Funding acquisition, Supervision, Validation.

Declaration of competing interest

The authors declare the following financial interests/personal relationships which may be considered as potential competing interests: Vikas Patil, Christoph Falter and Lukas Geissbühler are employed by the industrial partner that could have financial interests in the technology investigated by this article. The other authors do not have any known competing financial interests or personal relationships that could have appeared to influence the work reported in this paper.

Data availability

All critical data have been disclosed in the article and supplementary materials. For other data, please contact the corresponding author.

Acknowledgements

Supplementary data

Supplementary data to this article can be found online at https://doi.org/10.1016/j.scitotenv.2023.166005.

References

Ambrosetti, G., Good, P., 2019. A novel approach to high temperature solar receivers with an absorbing gas as heat transfer fluid and reduced radiative losses. Sol. Energy 183, 521–531. https://doi.org/10.1016/j.solener.2019.03.004.

Becattini, V., Gabrielli, P., Mazzotti, M., 2021. Role of carbon capture, storage, and utilization to enable a Net-Zero-CO_2-emissions aviation sector. Ind. Eng. Chem. Res. 60, 6848–6862. https://doi.org/10.1021/acs.iecr.0c05392.

Bos, M.J., Kersten, S.R.A., Brilman, D.W.F., 2020. Wind power to methanol: renewable methanol production using electricity, electrolysis of water and CO_2 air capture. Appl. Energy 264. https://doi.org/10.1016/j.apenergy.2020.114672.

Brendelberger, S., von Storch, H., Bulfin, B., Sattler, C., 2017. Vacuum pumping options for application in solar thermochemical redox cycles – assessment of mechanical-, jet- and thermochemical pumping systems. Sol. Energy 141, 91–102. https://doi.org/10.1016/j.solener.2016.11.023.

Brilman, W., 2020. CO_2 removal from air. In: Advances in Carbon Capture. Woodhead Publishing, pp. 523–543. https://doi.org/10.1016/B978-0-12-819657-1.00023-2.

Brown, A., Waldheim, L., Landälv, I., Saddler, J., Mahmood, E., McMillan, J.D., Bonomi, A., Klein, B., 2020. Advanced biofuels - potential for cost reduction. IEA Bioenergy 1–88.

Callegari, A., Bolognesi, S., Cecconet, D., Capodaglio, A.G., 2020. Production technologies, current role, and future prospects of biofuels feedstocks: a state-of-the-art review. Crit. Rev. Environ. Sci. Technol. 50, 384–436. https://doi.org/10.1080/10643389.2019.1629801.

Climeworks, 2022. Mammoth: a glimpse into the most advanced DAC+S facility steadily coming to life in winterly Iceland. URL. https://climeworks.com/news/climeworks-mammoth-construction-update-dec22?utm_source=LinkedIn&utm_medium=Social&utm_campaign=6 months mammoth&utm_content=mammothupdates. (Accessed 16 December 2022) (WWW Document).

Concawe, 2022. E-fuels: A Technoeconomic Assessment of European Domestic Production and Imports Towards 2050.

Corsi, C., Blanco, M.J., Grigoriev, V., Pye, J., 2022. Upper limits to the mean annual optical efficiency of solar mono-tower systems. Sol. Energy 236, 88–99. https://doi.org/10.1016/j.solener.2022.02.038.

de Jong, S., Hoefnagels, R., Faaij, A., Slade, R., Mawhood, R., Junginger, M., 2015. The feasibility of short-term production strategies for renewable jet fuels - a comprehensive techno-economic comparison. Biofuels Bioprod. Biorefin. https://doi.org/10.1002/bbb.1613.

de Klerk, A., 2011. Fischer-Tropsch Refining. Wiley. https://doi.org/10.1002/9783527635603.

Deutz, S., Bardow, A., 2021. Life-cycle assessment of an industrial direct air capture process based on temperature–vacuum swing adsorption. Nat. Energy 6, 203–213. https://doi.org/10.1038/s41560-020-00771-9.

Dieterich, V., Buttler, A., Hanel, A., Spliethoff, H., Fendt, S., 2020. Power-to-liquid *via* synthesis of methanol, DME or Fischer–Tropsch-fuels: a review. Energy Environ. Sci. 13, 3207–3252. https://doi.org/10.1039/D0EE01187H.

DOE, 2021. 2030 solar cost targets. URL. https://www.energy.gov/eere/solar/articles/2030-solar-cost-targets. (Accessed 24 October 2022) (WWW Document).

EC, 2018. Directive (EU) 2018/2001 of the European Parliament and of the Council of 11 December 2018 on the Promotion of the Use of Energy From Renewable Sources.

EC, 2023. Consumer Prices of Petroleum Products Net of Duties and Taxes.

EC JRC, 2023. JRC Photovoltaic Geographical Information System (PVGIS) - European Commission (WWW Document).

Ecoinvent, 2022. ecoinvent. URL. https://www.ecoinvent.org/. (Accessed 11 June 2022) (WWW Document).

Edwards, R., Padella, M., Giuntoli, J., Koeble, R., O'Connell, A., Bulgheroni, C., Marelli, L., 2017. Definition of Input Data to Assess GHG Default Emissions From Biofuels in EU Legislation, Version 1c. https://doi.org/10.2790/658143.

Ereev, S., Patel, M., 2012. Standardized cost estimation for new technologies (SCENT) methodology and tool. J. Bus. Chem. 9, 31.

Escobar, N., Laibach, N., 2021. Sustainability check for bio-based technologies: a review of process-based and life cycle approaches. Renew. Sust. Energ. Rev. https://doi.org/10.1016/j.rser.2020.110213.

EU, 2015. Directive 2015/652/EC of the European Parliament and of the Council of 20 April 2015 Laying Down Calculation Methods and Reporting Requirements Pursuant to Directive 98/70/EC and Relating to the Quality of Petrol and Diesel Fuels.

EU, 2023. Commission Delegated Regulation (EU) …/… of 10.2.2023 Supplementing Directive (EU) 2018/2001 of the European Parliament and of the Council by Establishing a Minimum Threshold for Greenhouse Gas Emissions Savings of Recycled Carbon Fuels and by Specifyin.

European Commission, 2016. Proposal for a Directive of the European Parliament and of the Council on the promotion of the use of energy from renewable sources. COM/2016/0767 final - 2016/0382 Off. J. Eur. Union.

Evans, S., 2017. The Swiss Company Hoping to Capture 1% of Global CO_2 Emissions by 2025. CarbonBrief.

Falter, C., Sizmann, A., 2022. Techno-economic analysis of solar thermochemical fuel production: sensitivity and uncertainty. AIP Conf. Proc. 2445 https://doi.org/10.1063/5.0085637.

Falter, C., Batteiger, V., Sizmann, A., 2016. Climate impact and economic feasibility of solar thermochemical jet fuel production. Environ. Sci. Technol. 50, 470–477. https://doi.org/10.1021/acs.est.5b03515.

Falter, C., Valente, A., Habersetzer, A., Iribarren, D., Dufour, J., 2020. An integrated techno-economic, environmental and social assessment of the solar thermochemical fuel pathway. Sustain. Energy Fuels 4, 3992–4002. https://doi.org/10.1039/D0SE00179A.

Fasihi, M., Efimova, O., Breyer, C., 2019. Techno-economic assessment of CO₂ direct air capture plants. J. Clean. Prod. 224, 957–980. https://doi.org/10.1016/j.jclepro.2019.03.086.

Frank, E.D., Elgowainy, A., Reddi, K., Bafana, A., 2021. Life-cycle analysis of greenhouse gas emissions from hydrogen delivery: a cost-guided analysis. Int. J. Hydrog. Energy 46, 22670–22683. https://doi.org/10.1016/j.ijhydene.2021.04.078.

Geissbühler, L., 2017. Thermocline Thermal Energy Storage: Advances and Applications to CSP, Compressed Air Energy Storage, and Solar Fuels. ETH Zurich.

Good, P., Ambrosetti, G., Furler, P., Geissbühler, L., Rutz, D., Ackermann, S., 2020. Invited talk: reaching beyond 1'500°C with the Synhelion absorbing gas solar receiver: results of experimental campaign. In: 2020 Virtual AIChE Annu. Meet. (WWW Document).

He, G., Lin, J., Sifuentes, F., Liu, X., Abhyankar, N., Phadke, A., 2020. Rapid cost decrease of renewables and storage accelerates the decarbonization of China's power system. Nat. Commun. 11 https://doi.org/10.1038/s41467-020-16184-x.

Holmes, H.E., Lively, R.P., Realff, M.J., 2021. Defining targets for adsorbent material performance to enable viable BECCS processes. JACS Au 1, 795–806. https://doi.org/10.1021/jacsau.0c00127.

IATA, 2022. IATA Economics' Chart of the Week Soaring Jet Fuel Prices Now Trending Downward.

IEA, 2020. Renewables 2020 Analysis and Forecast to 2025. Int. Energy Agency, p. 204. https://iea.blob.core.windows.net/assets/1a24f1fe-c971-4c25-964a-57d0f31eb97b/Renewables_2020-PDF.pdf.

IEA, 2022. Direct CO₂ emissions in the iron and steel sector by scenario, 2019–2050. URL. https://www.iea.org/data-and-statistics/charts/direct-co2-emissions-in-the-iron-and-steel-sector-by-scenario-2019-2050. (Accessed 14 January 2023).

Jones, S., Valkenburg, C., Walton, C., 2009. Production of Gasoline and Diesel From Biomass via Fast Pyrolysis, Hydrotreating and Hydrocracking: A Design Case. Pacific Northwest National Lab (PNNL) (doi:PNNL-22684.pdf).

JRC, CONCAWE, EUCAR, (JEC), 2014. Well-To-Wheels Report Version 4.a: Well-to Wheels Analysis of Future Automotive Fuels and Powertrains in the European Context.

Kim, A., Lee, H., Brigljević, B., Yoo, Y., Kim, S., Lim, H., 2021. Thorough economic and carbon footprint analysis of overall hydrogen supply for different hydrogen carriers from overseas production to inland distribution. J. Clean. Prod. 316 https://doi.org/10.1016/j.jclepro.2021.128326.

Kramer, D., 2018. Can carbon capture from air shift the climate change equation? Phys. Today 71, 26–29. https://doi.org/10.1063/PT.3.4018.

Kreutz, T.G., Larson, E.D., Elsido, C., Martelli, E., Greig, C., Williams, R.H., 2020. Techno-economic prospects for producing Fischer-Tropsch jet fuel and electricity from lignite and woody biomass with CO₂ capture for EOR. Appl. Energy 279. https://doi.org/10.1016/j.apenergy.2020.115841.

Kurup, P., Akar, S., Glynn, S., Augustine, C., Davenport, P., 2022. Cost update: commercial and advanced heliostat collectors. In: Natl. Renew. Energy Lab. NREL/TP-7A40-80482.

Leonzio, G., Fennell, P.S., Shah, N., 2022. A comparative study of different sorbents in the context of direct air capture (DAC): evaluation of key performance indicators and comparisons. Appl. Sci. 12 https://doi.org/10.3390/app12052618.

Lidor, A., Aschwanden, Y., Häseli, J., Reckinger, P., Haueter, P., Steinfeld, A., 2023. High-temperature heat recovery from a solar reactor for the thermochemical redox splitting of H₂O and CO₂. Appl. Energy 329, 120211. https://doi.org/10.1016/j.apenergy.2022.120211.

Lilliestam, J., Labordena, M., Patt, A., Pfenninger, S., 2017. Empirically observed learning rates for concentrating solar power and their responses to regime change. Nat. Energy 2. https://doi.org/10.1038/nenergy.2017.94.

Marchese, M., Marocco, P., Lanzini, A., Santarelli, M., 2022. Economic appraisal of Power-to-Liquid Fischer-Tropsch plants exploiting renewable electricity, green hydrogen, and CO₂ from biogas in Europe. E3S Web Conf. 334 https://doi.org/10.1051/e3sconf/202233402002.

Marur, P., Batra, R.C., Garcia, G., Loos, A.C., 2004. Static and dynamic fracture toughness of epoxy/alumina composite with submicron inclusions. J. Mater. Sci. 39, 1437–1440. https://doi.org/10.1023/B:JMSC.0000013912.58592.9e.

Methanex, 2023. About methanol-pricing. URL. https://www.methanex.com/about-methanol/pricing/. (Accessed 15 March 2023) (WWW Document).

Mishra, R., Ningthoujam, R.S., 2017. High-temperature Ceramics, Materials Under Extreme Conditions: Recent Trends and Future Prospects. Elsevier Inc. https://doi.org/10.1016/B978-0-12-801300-7.00011-5

Monnerie, N., Gan, P.G., Roeb, M., Sattler, C., 2020. Methanol production using hydrogen from concentrated solar energy. Int. J. Hydrog. Energy 45, 26117–26125. https://doi.org/10.1016/j.ijhydene.2019.12.200.

Moretti, C., 2023. Reflecting on the environmental impact of the captured carbon feedstock. Sci. Total Environ. 854 https://doi.org/10.1016/j.scitotenv.2022.158694.

Moretti, C., López-Contreras, A., de Vrije, T., Kraft, A., Junginger, M., Shen, L., 2021. From agricultural (by-)products to jet fuels: carbon footprint and economic performance. Sci. Total Environ. 775 https://doi.org/10.1016/j.scitotenv.2021.145848.

National Academies of Sciences, Engineering, and M, 2019. Negative Emissions Technologies and Reliable Sequestration. Negat. Emiss. Technol. Reliab. Sequestration A Res. Agenda. https://doi.org/10.17226/25259.

O'Connell, A., Kousoulidou, M., Lonza, L., Weindorf, W., 2019. Considerations on GHG emissions and energy balances of promising aviation biofuel pathways. Renew. Sust. Energ. Rev. https://doi.org/10.1016/j.rser.2018.11.033.

Onigbajumo, A., Swarnkar, P., Will, G., Sundararajan, T., Taghipour, A., Couperthwaite, S., Steinberg, T., Rainey, T., 2022. Techno-economic evaluation of solar-driven ceria thermochemical water-splitting for hydrogen production in a fluidized bed reactor. J. Clean. Prod. 371 https://doi.org/10.1016/j.jclepro.2022.133303.

Panlener, R.J., Blumenthal, R.N., Garnier, J.E., 1975. A thermodynamic study of nonstoichiometric cerium dioxide. J. Phys. Chem. Solids 36, 1213–1222.

Poluzzi, A., Guandalini, G., Guffanti, S., Martinelli, M., Moioli, S., Huttenhuis, P., Rexwinkel, G., Palonen, J., Martelli, E., Groppi, G., Romano, M.C., 2022. Flexible power and biomass-to-methanol plants with different gasification technologies. Front. Energy Res. 9 https://doi.org/10.3389/fenrg.2021.795673.

Prats-Salvado, E., Monnerie, N., Sattler, C., 2021. Synergies between direct air capture technologies and solar thermochemical cycles in the production of methanol. Energies 14. https://doi.org/10.3390/en14164818.

Prats-Salvado, E., Monnerie, N., Sattler, C., 2022. Techno-economic assessment of the integration of direct air capture and the production of solar fuels. Energies 15. https://doi.org/10.3390/en15145017.

Reinert, C., Deutz, S., Minten, H., Dörpinghaus, L., von Pfingsten, S., Baumgärtner, N., Bardow, A., 2021. Environmental impacts of the future German energy system from integrated energy systems optimization and dynamic life cycle assessment. Comput. Chem. Eng. 153 https://doi.org/10.1016/j.compchemeng.2021.107406.

Renewable fuels association, 2022. Annual ethanol production U.S. and world ethanol production. URL. https://ethanolrfa.org/markets-and-statistics/annual-ethanol-production. (Accessed 8 March 2023) (WWW Document).

Schäppi, R., Rutz, D., Dähler, F., Muroyama, A., Haueter, P., Lilliestam, J., Patt, A., Furler, P., Steinfeld, A., 2022. Drop-in fuels from sunlight and air. Nature 601, 63–68. https://doi.org/10.1038/s41586-021-04174-y.

Sinha, A., Realff, M.J., 2019. A parametric study of the techno-economics of direct CO₂ air capture systems using solid adsorbents. AICHE J. 65 https://doi.org/10.1002/aic.16607.

Skorikova, G., Saric, M., Sluijter, S.N., van Kampen, J., Sánchez-Martínez, C., Boon, J., 2020. The techno-economic benefit of sorption enhancement: evaluation of sorption-enhanced dimethyl ether synthesis for CO₂ utilization. Front. Chem. Eng. 2 https://doi.org/10.3389/fceng.2020.594884.

SkyNRG, 2023. Book & Claim explained: what is Book and Claim? URL. https://skynrg.com/book-claim-explained-what-is-book-and-claim/. (Accessed 30 March 2023) (WWW Document).

Terlouw, T., Treyer, K., Bauer, C., Mazzotti, M., 2021. Life cycle assessment of direct air carbon capture and storage with low-carbon energy sources. Environ. Sci. Technol. 55, 11397–11411. https://doi.org/10.1021/acs.est.1c03263.

Thornton, G., 2019. Renewable Energy Discount Rate Survey Results – 2018.

Trinca, A., Bassano, C., Verdone, N., Deiana, P., Vilardi, G., 2023. Modelling and economic evaluation of CCS/PtX technologies integrated into biomass MTG plants. J. Environ. Chem. Eng. 11 https://doi.org/10.1016/j.jece.2022.109184.

Tsongidis, N.I., Asimakopoulou, A.G., Pantoleontos, G., Konstandopoulos, A.G., 2019. Transportation and solar-aided utilization of CO₂: technoeconomic analysis of spanning routes of CO₂ conversion to solar fuels. J. CO2 Util. 30, 142–157. https://doi.org/10.1016/j.jcou.2019.01.010.

U.S. DoE, 2017. The SunShot 2030 Goals. Sol. Energy Technol. Off. U.S. Dep. Energy, USA, pp. 1–5.

Wijesiri, R.P., Knowles, G.P., Yeasmin, H., Hoadley, A.F.A., Chaffee, A.L., 2019. Technoeconomic evaluation of a process capturing CO₂ directly from air. Processes 7. https://doi.org/10.3390/PR7080503.

Wurzbacher, J.A., Gebald, C., Piatkowski, N., Steinfeld, A., 2012. Concurrent separation of CO₂ and H₂O from air by a temperature-vacuum swing adsorption/desorption cycle. Environ. Sci. Technol. 46, 9191–9198. https://doi.org/10.1021/es301953k.

Yu, Q., Delgado, J.D.L.P., Veneman, R., Brilman, D.W.F., 2017. Stability of a benzyl amine based CO₂ capture adsorbent in view of regeneration strategies. Ind. Eng. Chem. Res. 56, 3259–3269. https://doi.org/10.1021/acs.iecr.6b04645.

Zang, G., Sun, P., Elgowainy, A.A., Bafana, A., Wang, M., 2021. Performance and cost analysis of liquid fuel production from H₂ and CO₂ based on the Fischer-Tropsch process. J. CO2 Util. 46 https://doi.org/10.1016/j.jcou.2021.101459.

Zanganeh, G., Pedretti, A., Zavattoni, S., Barbato, M., Steinfeld, A., 2012. Packed-bed thermal storage for concentrated solar power - pilot-scale demonstration and industrial-scale design. Sol. Energy 86, 3084–3098. https://doi.org/10.1016/j.solener.2012.07.019.

Zoller, S., Koepf, E., Nizamian, D., Stephan, M., Patané, A., Haueter, P., Romero, M., González-Aguilar, J., Lieftink, D., de Wit, E., Brendelberger, S., Sizmann, A., Steinfeld, A., 2022. A solar tower fuel plant for the thermochemical production of kerosene from H₂O and CO₂. Joule 6, 1606–1616. https://doi.org/10.1016/j.joule.2022.06.012.